Appendix 1

Keplerian orbits

This appendix reviews the key properties of Keplerian orbits; that is, orbits that result from the solution of the Newtonian equations of motion with a central, attractive, inverse square field. Perturbations to such motion are not considered here.

A1.1 GEOMETRY OF CONIC SECTIONS

Keplerian orbits may be expressed in terms of conic sections. Therefore, the geometry of such entities is of some importance.

The ellipse is shown in Figure A1.1.

The following relationships are used in describing orbits:

- Semi-major axis, a.
- Semi-minor axis, b.
- Semi-minor axis, p.
- Eccentricity, e.

The geometry of an ellipse is such that:

$$\frac{x^2}{a^2} + \frac{y^2}{b^2} = 1$$

It may be seen that $b = a\sqrt{(1 - e^2)}$, and that $p = a(1 - e^2)$.

In the case of an ellipse, the eccentricity is such that $0 \leq e < 1$. In the case of the hyperbola, the geometry is shown in Figure A1.2.

Two solutions are possible for the hyperbola, such that in the figure the mirror image about a vertical axis through the origin gives the second solution.

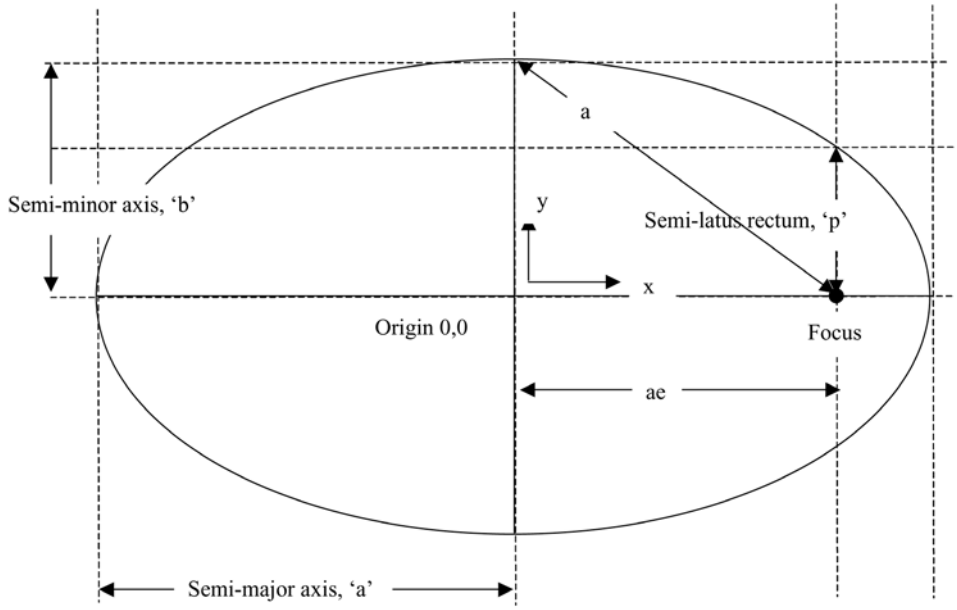

Figure A1.1. Geometry of the ellipse.

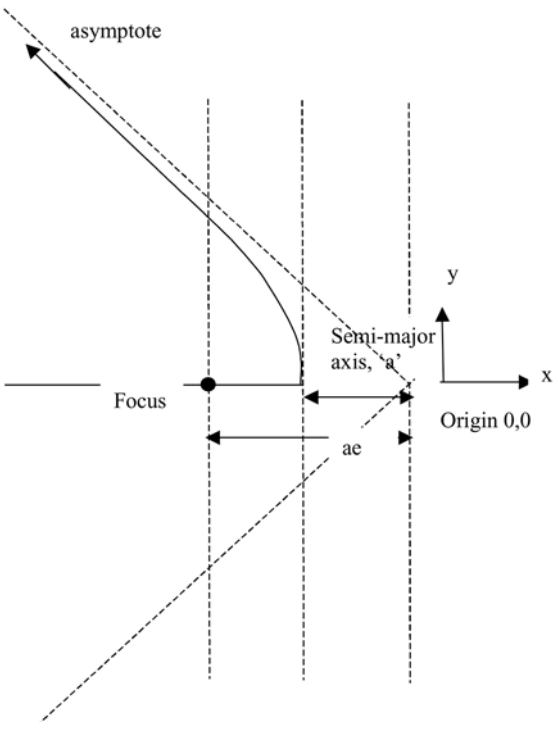

Figure A1.2. Section of a hyperbola.

The geometry of an hyperbola is such that:

$$\frac{x^2}{a^2} - \frac{y^2}{b^2} = 1$$

where $b^2 = a^2(e^2 - 1)$.

The eccentricity is such that: $e > 1$.

A1.2 SUMMARY OF ORBIT NOTATIONS

The following elements are conventionally used to describe the orbit of a spacecraft. The origin of the reference frame is assumed to be the centre of the central body under consideration. A reference plane is assumed. In the case of motion about the Sun, the plane of the ecliptic is taken as the reference. For Earth-relative motion the equator is used. A more detailed discussion on reference systems may be found in Appendix 2.

- a = semi-major axis of the orbit ellipse.
- e = eccentricity of the orbit ($e = 0$ for circular orbits).
- i = inclination of orbit with respect to the equatorial plane or reference plane.
- Ω = right ascension of ascending node.
- ω = argument of perigee.
- θ = true anomaly of satellite.

The central body lies at the focus of the ellipse or hyperbola.

Figure A1.3 illustrates the orbital elements used to describe the plane of a satellite orbit:

The ascending node is defined by the point where the spacecraft passes through the reference plane, in a northerly direction (i.e., positive velocity component in the z or 'polar' direction). It is measured from the reference axis X direction. This is often nominally the 'first point of Aries'. The right ascension is the angle in the reference plane between X and the ascending node. Further definitions related to this idea are the descending node, where the spacecraft moves through the reference plane in a southerly direction, and the anti-node, where the latitude of the spacecraft's motion reaches its maximum or minimum values. Inclination is measured as the rotation about the ascending node from the reference plane to the orbit plane (positive rotation in Figure A1.3). The inclination vector is a vector normal to the orbit plane and a rotation about this vector is in the direction of the orbit of the spacecraft. In Figure A1.3, the projection of the orbit into the reference plane is drawn as the lighter line.

In Figure A1.4 the argument of pericentre is the angle in the orbit plane measured from the ascending node to the pericentre. It is a rotation about the inclination vector (positive rotation in Figure A1.4). In this figure the projection of the orbit into the reference plane is drawn as the lighter line. Pericentre is the point of closest approach, and the apocentre the extreme point in the orbit. The apocentre seen in the figure therefore lies below the reference plane (Earth equatorial plane in

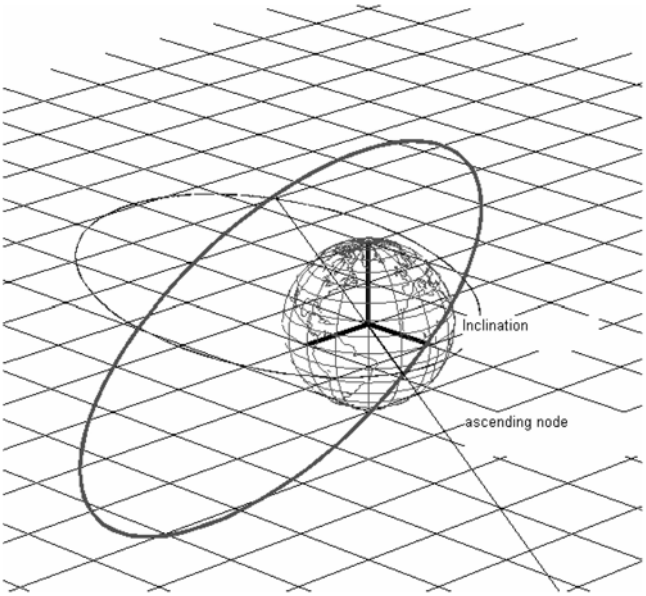

Figure A1.3. Inclination and the ascending node. The light dashed line is the projection of the orbit into the reference plane.

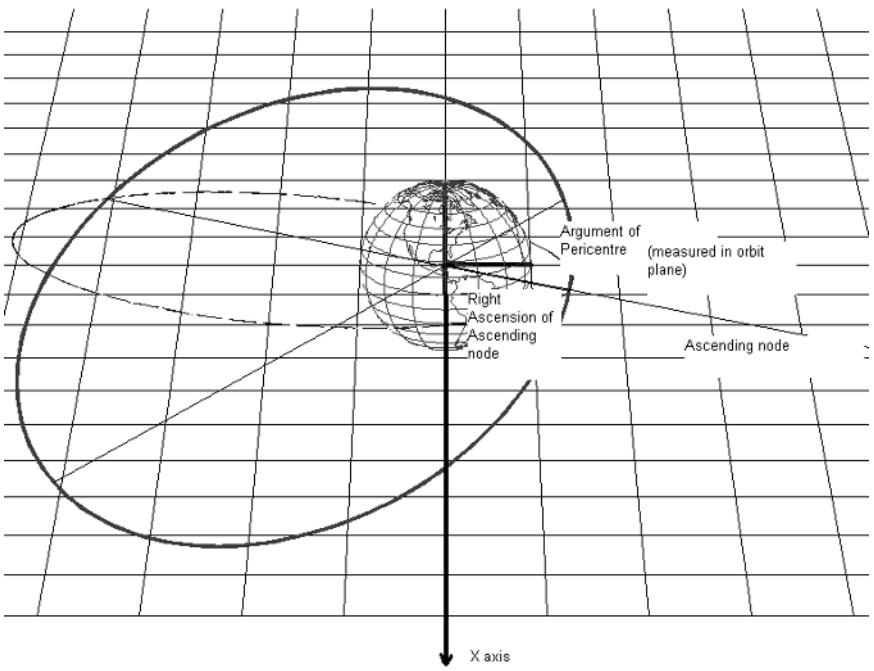

Figure A1.4. Right ascension and argument of pericentre. The light dashed line is the projection of the orbit into the reference plane.

this example). The true anomaly of the orbiting body is the angle, measured in the orbit plane, between the pericentre and its current location. Note that alternative representations of the location in the orbit are possible. In this previous definition, true anomaly is used.

Alternatively, mean anomaly can be used. In the case of a bound orbit, mean anomaly describes the fraction of an orbital period since the subject passed pericentre. It takes values in the range 0 to 2π. One period is completed when mean anomaly is incremented by 2π. A useful quantity associated with mean anomaly is the mean motion, n:

$$n = \sqrt{\frac{\mu}{a^3}} \tag{1.1}$$

such that the orbit period is expressed as:

$$\tau = \frac{2\pi}{n} \tag{1.2}$$

where μ is the gravitational parameter of the central body.

To calculate true anomaly from mean anomaly, when the eccentricity of the orbit is less than 1, an intermediate variable, the eccentric anomaly, is required. This angle is illustrated geometrically in Figure A1.5.

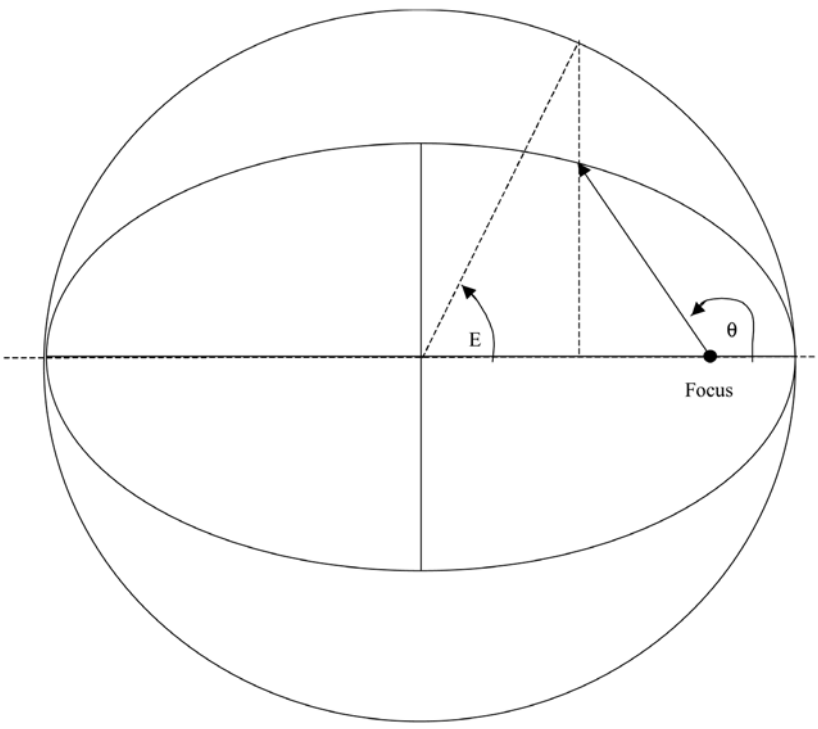

Figure A1.5. Eccentric anomaly.

The relationship between the two quantities is the following:

$$M = E - e\sin E \tag{1.3}$$

where M is mean anomaly and E is eccentric anomaly. This is known as Kepler's equation, which may not be solved analytically for E. An iterative solution is therefore employed. A Newton–Raphson method may be used as follows:

$$M' = E - e\sin E$$

where M' is the current evaluation of mean anomaly given the estimate, E of the eccentric anomaly.

$$E = E + \frac{(M - M')}{\dfrac{\partial M}{\partial E}} \qquad \text{and} \qquad \frac{\partial M}{\partial E} = 1 - e\cos E \tag{1.4}$$

Various schemes have been devised for the solution of the above equation, of which this particular iterative method is only one. The equation may present numerical difficulties when eccentricity approaches 1. A detailed discussion may be found in Battin (see references).

True anomaly is obtained by:

$$\tan\frac{\theta}{2} = \sqrt{\frac{1+e}{1-e}}\tan\frac{E}{2} \tag{1.5}$$

Alternative expressions for the relationship between true and eccentric anomalies are:

$$\cos\theta = \frac{\cos E - e}{1 - e\cos E} \qquad \text{and} \qquad \sin\theta = \frac{\sin E\sqrt{1-e^2}}{1 - e\cos E} \tag{1.6}$$

In the case of a hyperbolic orbit, where the eccentricity exceeds 1, the mean anomaly is converted to true anomaly by use of an intermediate variable known as the hyperbolic anomaly. The relationship between the two quantities is the following:

$$M = e\sinh F - F \tag{1.7}$$

where M is mean anomaly and F is hyperbolic anomaly. An iterative solution is again employed, using the Newton–Raphson method as follows:

$$M' = e\sinh F - F$$

where M' is the current evaluation of mean anomaly given the estimate, F of the hyperbolic anomaly:

$$F = F + \frac{(M - M')}{\dfrac{\partial M}{\partial F}} \qquad \text{and} \qquad \frac{\partial M}{\partial F} = e\cosh F - 1$$

The true anomaly is now obtained from:

$$\tan\frac{\theta}{2} = \sqrt{\frac{e+1}{e-1}}\tanh\frac{F}{2} \tag{1.8}$$

A special case exists for the parabola, where eccentricity is equal to 1. In this situation, Barker's equation gives the relationship between true anomaly and time.

Non-singular elements

It can be seen that the previous expressions are singular. When the inclination is zero, the ascending node is not well defined. When the eccentricity is zero and therefore the orbit circular, the pericentre is not well defined.

To alleviate these problems, non-singular elements may be used to describe the orbit. The elements e, i, ω and Ω are replaced as follows:

$$P_1 = e\sin(\Omega + \omega)$$
$$P_2 = e\cos(\Omega + \omega) \tag{1.9}$$

$$Q_1 = \tan\left(\frac{i}{2}\right)\sin\Omega$$
$$Q_2 = \tan\left(\frac{i}{2}\right)\cos\Omega \tag{1.10}$$

Furthermore, the 'true longitude' can also be used, being defined as:

$$L = \omega + \Omega + \theta \tag{1.11}$$

It should be noted that this is not a 'real' longitude with a physical meaning; the right ascension of the ascending node lies in a different plane to the argument of pericentre and true anomaly. It is a mathematical construction of convenience.

The transformation to conventional elements is given by:

$$e^2 = P_1^2 + P_2^2$$
$$\tan^2\left(\frac{i}{2}\right) = Q_1^2 + Q_2^2$$
$$\tan\Omega = \frac{Q_1}{Q_2}$$
$$\tan(\omega + \Omega) = \frac{P_1}{P_2}$$

Such forms are useful when considering the effects of perturbing forces on orbits close to the singular values. The evolution of the non-singular elements can be monitored in preference to classical elements.

A1.3 MOTION IN AN ATTRACTIVE CENTRAL INVERSE SQUARE FIELD

The motion of a body under the influence of an inverse-square attractive field may be analysed to obtain analytical expressions for the motion. This motion is often referred to as the solution of the two body problem, or Keplerian motion. It is the motion to which Kepler's laws apply.

The gravitational force exerted on a body of mass m_2 by a body of mass, m_1 is given by:

$$m_2\ddot{\underline{r}}_2 = -\frac{Gm_1m_2\underline{r}}{r^3} \tag{1.12}$$

where $\underline{r}$ is the vector from the centre of mass of the body 1 to the centre of mass of the body, 2, and $\underline{r_2}$ is the vector from the centre of mass of the system (i.e., body 1 plus body 2) to body 2. Similarly:

$$m_1\ddot{\underline{r}}_1 = \frac{Gm_1m_2\underline{r}}{r^3} \tag{1.13}$$

where $\underline{r_1}$ is the vector from the centre of mass of the system to body 1.

The acceleration of body 2 relative to body 1 is given by:

$$\ddot{\underline{r}} = -\frac{G(m_1+m_2)\,\underline{r}}{r^3} \tag{1.14}$$

In the following it will now be assumed that body 1 is much more massive than body 2. The gravitational constant for this body is defined as: $\mu = Gm_1$:

$$\ddot{\underline{r}} = -\frac{(m_1+m_2)}{m_1}\frac{\mu\underline{r}}{r^3} \qquad \text{or} \qquad \frac{m_1m_2}{(m_1+m_2)}\,\ddot{\underline{r}} = -m_2\frac{\mu\underline{r}}{r^3} \tag{1.15}$$

where $\dfrac{m_1m_2}{(m_1+m_2)}$ is sometimes referred to as the 'reduced' mass.

If the mass of body 2 can be neglected in comparison with body 1, the subscript 2 will be omitted when referring to the motion of the spacecraft.

Then equation 1.15 becomes the following:

$$\ddot{\underline{r}} = -\frac{\mu\underline{r}}{r^3} \tag{1.16}$$

The force acting only along the separation of the two bodies means that:

$$\underline{r} \wedge m\ddot{\underline{r}} = 0$$

and therefore a constant of motion is the angular momentum of the spacecraft, $\underline{h}$:

$$\underline{r} \wedge m\dot{\underline{r}} = \text{constant} = \underline{h} \tag{1.17}$$

Therefore, the motion remains in the same plane. This conclusion allows a simplification to be made in the description of the motion such that polar co-ordinates (r, θ) can be used. Then:

$$\underline{V} = \dot{\underline{r}} = \dot{r}\hat{r} + r\dot{\theta}\hat{\theta} \tag{1.18}$$

$$V^2 = \dot{r}^2 + r^2\dot{\theta}^2 \tag{1.19}$$

where $\hat{r}$, $\hat{\theta}$ are unit vectors in the radial and transverse directions respectively, and:

$$h = mr^2\dot{\theta} \tag{1.20}$$

The energy of body 2 is given by the sum of potential and kinetic energies:

$$E = \frac{m}{2}(\dot{r}^2 + r^2\dot{\theta}^2) - \frac{Gm_1m}{r} \tag{1.21}$$

Using equation 1.21 it is possible to derive further information regarding the motion of body 2. Substituting for angular momentum gives:

$$E = \frac{m\dot{r}^2}{2} + \frac{h^2}{2mr^2} - \frac{\mu m}{r} \tag{1.22}$$

where $\mu = Gm_1$. Then, using equation 1.20 and equation 1.22

$$\left(\frac{dr}{d\theta}\right)^2 = \frac{r^2}{h^2}(2Emr^2 + 2\mu m^2 r - h^2) \tag{1.23}$$

In the following, the expressions for energy and angular momentum will be used as those relating to unit mass, $m = 1$, or 'specific energy' and 'specific angular momentum':

$$\left(\frac{dr}{d\theta}\right)^2 = \frac{r^2}{h^2}(2Er^2 + 2\mu r - h^2) \qquad \text{and} \qquad h = r^2\dot{\theta}$$

which may be integrated to give:

$$\frac{1}{r} = \frac{\mu}{h^2}\left(1 + \sqrt{1 + \frac{2Eh^2}{\mu^2}}\cos(\theta - \theta_0)\right) \tag{1.24}$$

where θ_0 is a constant. This is the equation of a conic section with eccentricity given by:

$$e = \sqrt{1 + \frac{2Eh^2}{\mu^2}} \tag{1.25}$$

The point of closest approach occurs when $\theta = \theta_0$. This is the pericentre of the orbit, and the true anomaly may be substituted for $\theta - \theta_0$.

The semi-major axis can be shown to be given by:

$$a = -\frac{\mu}{2E} \tag{1.26}$$

The semi-latus rectum is defined geometrically as:

$$p = a(1 - e^2) \tag{1.27}$$

and is therefore:

$$p = \frac{h^2}{\mu} \tag{1.28}$$

such that:

$$r = \frac{p}{(1 + e\cos(\theta))} = \frac{a(1 - e^2)}{(1 + e\cos(\theta))} \tag{1.29}$$

where θ is used to represent the angle measured in the orbit plane from pericentre, previously denoted as $\theta - \theta_0$.

The relationship between velocity and radius is found through the energy per unit mass:

$$E = \frac{V^2}{2} - \frac{\mu}{r}$$

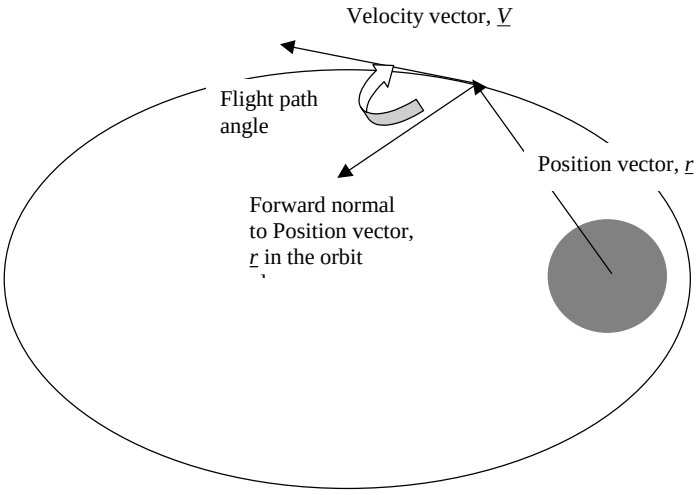

Figure A1.6. Flight path angle geometry.

and therefore

$$V = \sqrt{2\mu\left(\frac{1}{r} - \frac{1}{2a}\right)} \tag{1.30}$$

The direction of the velocity with respect to the forward normal to the radius vector (Figure A1.6) is defined by the flight path angle. This is obtained from the radial velocity component:

$$V \sin \Gamma = \left(e \sin \theta \sqrt{\frac{\mu}{a(1-e^2)}}\right) \tag{1.31}$$

Also, the velocity component V_θ is given by h/r, and an alternative expression for flight path angle is:

$$\tan \Gamma = \frac{V_r}{V_\theta} = \frac{V \sin \Gamma}{V \cos \Gamma} = \frac{e \sin \theta}{1 + e \cos \theta} \tag{1.32}$$

Therefore, the flight path angle depends only on eccentricity and true anomaly. Three cases of eccentricity may be considered.

$0 \leq e < 1$: elliptical orbits
$e = 1$: parabolic orbits
$e > 1$: hyperbolic orbits

If the eccentricity exceeds 1, the energy is positive and the spacecraft will depart from the central body under consideration. Conversely, with an eccentricity of less than 1 the energy is negative and the spacecraft remains in a closed orbit. In the special case of eccentricity being equal to 1, the result is a parabolic orbit and zero energy. The spacecraft reaches zero velocity at infinite distance from the central body.

In the cases of hyperbolic orbits, additional parameters of interest may be

evaluated as follows. The first is the excess hyperbolic speed – the speed remaining when the spacecraft reaches infinite distance from the central body under consideration:

$$V_\infty^2 = -\frac{\mu}{a} = 2E \tag{1.33}$$

The escape velocity may be defined as the speed, when at a given radial distance from the planet, with which the spacecraft achieves a positive energy:

$$V^2 \geq 2\frac{\mu}{r} \tag{1.34}$$

If it is in an initial circular orbit about the planet, then:

$$V^2 \geq 2\frac{\mu}{a}$$

A1.4 GENERATION OF CARTESIAN CO-ORDINATES FROM ORBITAL ELEMENTS

Given an orbit ephemeris, it is possible to derive a set of Cartesian co-ordinates and a velocity vector. The Cartesian position and velocity vector are an alternative representation of the instantaneous state of an orbit (six components are required to represent the state).

Cartesian co-ordinates are illustrated in Figure A1.7.

The procedure for conversion of ephemeris to Cartesian co-ordinates is as follows. The radial distance is given by:

$$r = a\frac{(1-e^2)}{(1+e\cos\theta)}$$

(using the same rotation as the previous section, A1.3)

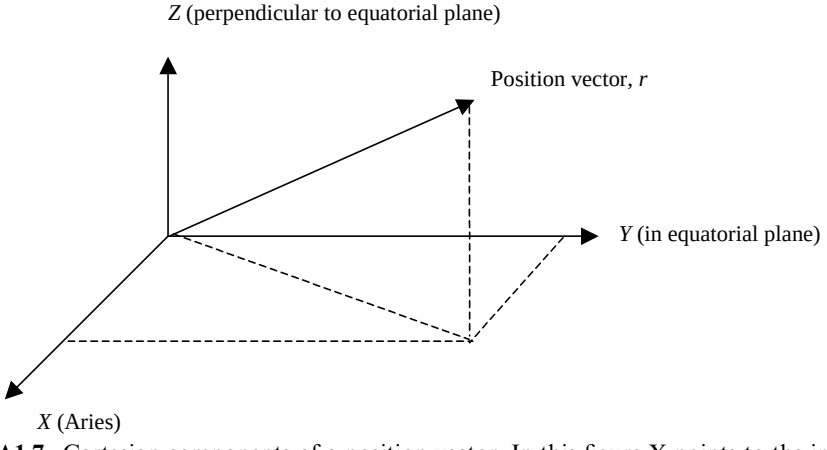

Figure A1.7. Cartesian components of a position vector. In this figure X points to the inertial reference direction.

The speed is given by

$$V = \sqrt{2\mu\left(\frac{1}{r} - \frac{1}{2a}\right)}$$

where μ is the central body gravitational parameter.

X, Y and Z components of the position vector are calculated in an intermediate reference frame (X' lies in the equatorial plane and the orbit plane, along the direction of the ascending node, Y' lies in the equatorial plane, and Z' completes the right-handed set, being perpendicular to the equatorial plane):

$$\begin{aligned} r'_x &= r\cos(\omega + \theta) \\ r'_y &= r\sin(\omega + \theta) * \cos i \\ r'_z &= r\sin(\omega + \theta) * \sin i \end{aligned} \tag{1.35}$$

These co-ordinates are now calculated with respect to an axis set with X pointing to Aries, Y perpendicular to X in the equatorial plane, and Z unchanged:

$$\begin{aligned} r_x &= r'_x\cos(\Omega) - r'_y\sin(\Omega) \\ r_y &= r'_x\sin(\Omega) + r'_y\cos(\Omega) \\ r_z &= r'_z \end{aligned} \tag{1.36}$$

The Cartesian co-ordinates are therefore obtained.

The flight path angle (the angle between the velocity vector and the normal to the radius vector, in the orbit plane) is given by:

$$\Gamma = \sin^{-1}\left(e\frac{\sin\theta}{V}\sqrt{\frac{\mu}{a(1-e^2)}}\right) \qquad \text{or} \qquad \Gamma = \tan^{-1}\left(\frac{e\sin\theta}{1+e\cos\theta}\right) \tag{1.37}$$

The velocity vector components calculated in the intermediate reference frame are:

$$\begin{aligned} V'_x &= V\cos\left(\omega + \theta + \frac{\pi}{2} - \Gamma\right) \\ V'_y &= V\sin\left(\omega + \theta + \frac{\pi}{2} - \Gamma\right)\sin i \\ V'_z &= V\sin\left(\omega + \theta + \frac{\pi}{2} - \Gamma\right)\cos i \end{aligned} \tag{1.38}$$

These components are now calculated with respect to an axis set with X pointing to Aries, Y perpendicular to X in the equatorial plane, and Z unchanged:

$$\begin{aligned} V_x &= V'_x\cos(\Omega) - V'_y\sin(\Omega) \\ V_y &= V'_x\sin(\Omega) + V'_y\cos(\Omega) \\ V_z &= V'_z \end{aligned} \tag{1.39}$$

A1.5 GENERATION OF ORBITAL ELEMENTS FROM CARTESIAN COMPONENTS

The six orbital elements can be derived from the Cartesian state vector (three position and three velocity vector components). Firstly, the angular momentum is calculated (assuming unit mass) from the relationship:

$$\underline{h} = \underline{r} \wedge \underline{V} \tag{1.40}$$

where $\underline{r}$ and $\underline{V}$ are the position and velocity vectors and therefore $h^2 = h_x^2 + h_y^2 + h_Z^2$, where h_x, h_y and h_z are the components in x, y, and z directions.

This is used to find the inclination and right ascension of ascending node. The location of the ascending node is given by:

$$\Omega = \tan^{-1}\left(\frac{h_x}{-h_y}\right) \tag{1.41}$$

and the inclination is given by:

$$i = \tan^{-1}\left(\frac{\sqrt{h_x^2 + h_y^2}}{h_z}\right) \tag{1.42}$$

The Laplace–Range–Lenz vector may now be obtained as follows:

$$\underline{E} = \underline{V} \wedge \underline{h} - \frac{\mu \underline{r}}{r} \tag{1.43}$$

and $E = \sqrt{E_x^2 + E_y^2 + E_z^2} = \mu e$.

The Laplace–Range–Lenz vector allows the calculation of the argument of pericentre, which is now calculated from:

$$\sin\omega = \frac{E_z}{E \sin i} \quad \text{for } i \neq 0 \tag{1.44}$$

$$\cos\omega = \frac{E_x + E \sin\omega \cos i \sin\Omega}{E \cos\Omega} \tag{1.45}$$

$$\omega = \tan^{-1}\left(\frac{\sin\omega}{\cos\omega}\right) \tag{1.46}$$

This formulation allows the pericentre to be located correctly over a 360-degree range.

The semi-major axis is calculated from the orbital energy. Then,

$$Energy = \frac{V^2}{2} - \frac{\mu}{r}$$

giving

$$a = \frac{-\mu}{2Energy} \tag{1.47}$$

The eccentricity is now obtained by:

$$e = \sqrt{1 + 2Energy\left(\frac{h}{\mu}\right)^2} \tag{1.48}$$

Having obtained the main orbital parameters, the location within the orbit is given by the true anomaly, which may be obtained geometrically by using an intermediate transformation:

$$r'_x = r_x \cos\Omega + r_y \sin\Omega$$
$$r'_y = r_y \cos\Omega - r_x \sin\Omega$$
$$r''_y = r'_y \cos i + r_z \sin i \tag{1.49}$$

Then

$$\sin\theta = \frac{r''_y \cos\omega - r'_x \sin\omega}{r} \tag{1.50}$$

$$\cos\theta = \frac{r''_y \sin\omega + r'_x \cos\omega}{r} \tag{1.51}$$

and $\theta = \tan^{-1}\left(\dfrac{\sin\theta}{\cos\theta}\right)$. This formulation allows the true anomaly to be located correctly over a 360-degree range.

If $e < 1$, the mean anomaly is calculated using the eccentric anomaly:

$$\cos E = \frac{e + \cos\theta}{1 + e\cos\theta} \tag{1.52}$$

and

$$\sin E = \frac{\sin\theta(1 - e\cos E)}{\sqrt{1 - e^2}} \tag{1.53}$$

then $E = \tan^{-1}\left(\dfrac{\sin E}{\cos E}\right)$ and $M = E - e\sin E$.

If $e > 1$, the mean anomaly is calculated via the hyperbolic anomaly, F:

$$F = 2\tan^{-1}\left(\tan\left(\frac{\theta}{2}\right)\sqrt{\frac{e-1}{e+1}}\right) \tag{1.54}$$

and

$$M = -F + e\sinh F \tag{1.55}$$

Appendix 2

Frames of reference

Our Galaxy is one of many in a rapidly expanding Universe. Within our Galaxy the Sun moves at a velocity of approximately 250 km/sec with respect to the Galactic centre. However, when considering the motion of spacecraft executing interplanetary transfers, these velocities are not considered, as the key reference point for motion is the Sun. The gravitational forces exerted by distant objects outside the Solar System are small, and usually need not be considered. Furthermore, because of their great distances they impart a near-constant acceleration on all of the bodies within our Solar System; that is, the gravity gradient is so small that differential acceleration terms are negligible.

A2.1 REFERENCE AXES

The usual origin considered for motion within the Solar System is referenced to the centre of the Sun. An inertially oriented axis set is used. A reference plane is defined, being the ecliptic. This plane contains the Sun and the Earth's orbit. However, as the Earth's orbital plane is perturbed by the other planets of the Solar System, such a plane would very slowly change its orientation with time. Therefore, the ecliptic is often referred to that pertaining at a particular reference epoch.

Within the ecliptic plane exists a reference direction, nominally aligned with the direction of a distant star, the first point in the constellation of Aries. Such a celestial alignment is chosen as it defines a near fixed, inertial direction. This direction defines the X axis direction of a reference frame, and is chosen as it lies very close to the direction of the Sun, as seen from Earth, at the northern hemisphere Spring or Vernal Equinox (21 March). It therefore lies along the intersection of the Earth's equatorial plane with the ecliptic. However, this direction also shows a small drift over time and is again referenced to a particular epoch (discussed subsequently). The second, Y, axis is chosen to lie in the ecliptic plane, and is orthogonal to X. This

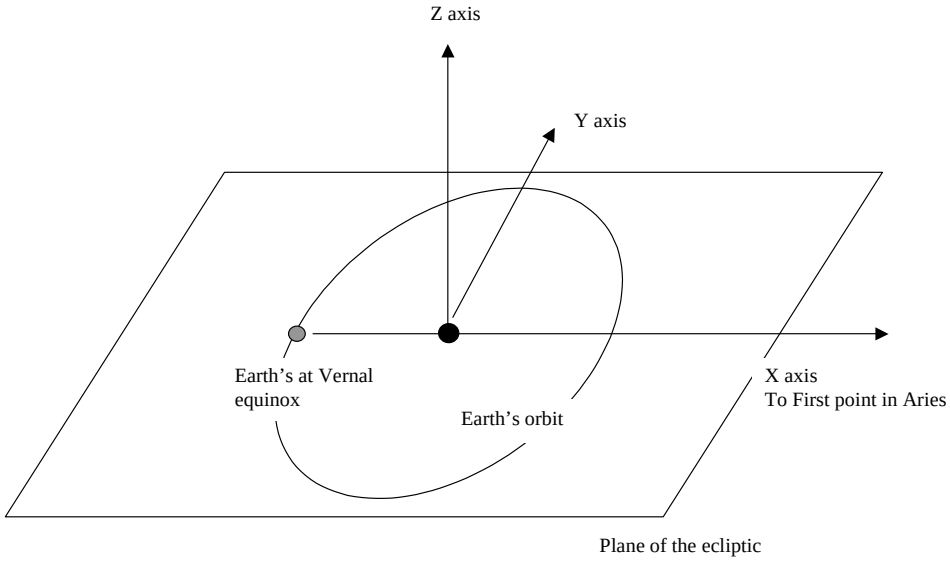

Figure A2.1. Reference axes in the ecliptic plane.

means that the right-handed axis set is completed by Z, which is perpendicular to the ecliptic. The ambiguity of this choice is removed by relating this direction to the direction of a celestial pole. Also, the choice of X and Y axes (as a rotation about the Z axis from X to Y) is consistent with the direction of the rotation of the planets about the Sun. This is sometimes considered to be an 'inertial' reference set. It is inertial in the sense that its direction is fixed inertially, although its origin in this case moves with the centre of the Sun, which is accelerated by the other planets of the Solar System and (as discussed previously) by bodies outside the Solar System. The axis set is illustrated in Figure A2.1.

Further frames of reference are used when motion with respect to a particular planet is considered. The natural choice for the X–Y plane is the planet's equatorial plane. In Earth's case, the X axis again lies in the direction of Aries, which is contained both within the ecliptic plane and Earth's equatorial plane. As in the case of the ecliptic plane, Earth's equatorial plane does not remain fixed, but experiences a small motion over long periods of time. Therefore, as in the ecliptic case, its orientation may be defined at a reference epoch.

The relationship between equatorial and ecliptic axes is defined by the inclination of the ecliptic with respect to the Earth's equatorial plane, otherwise known as the obliquity of the ecliptic. This is illustrated in Figure A2.2.

Drift in the reference directions

The X direction has been chosen to correspond to the intersection of the ecliptic and equatorial planes. This corresponded to the direction of the first point of Aries approximately 2,000 years ago. The intersection of the two planes slowly changes

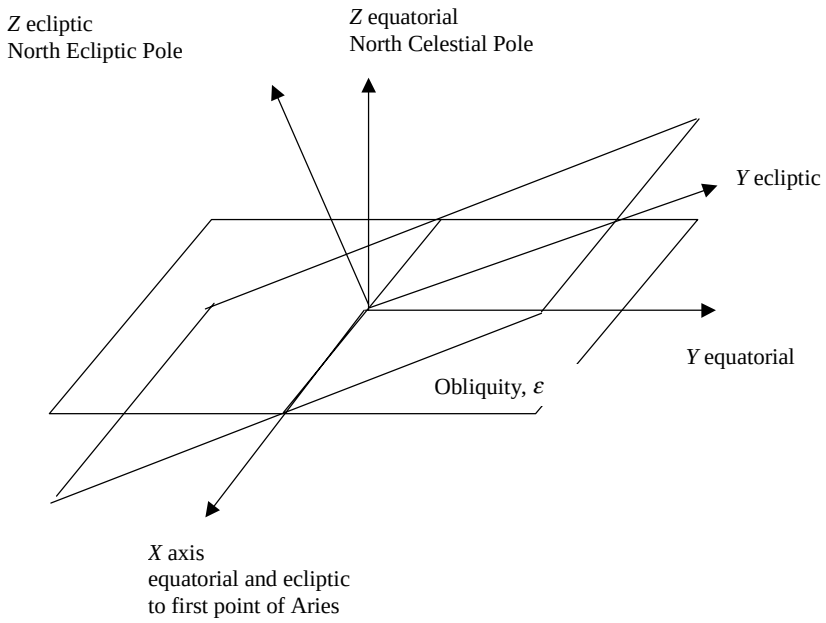

Figure A2.2. Relationship between ecliptic and Earth equatorial planes.

because of a precession and nutation of the Earth's axis of rotation, and also because of a slow change in the orientation of the plane of the ecliptic.

An axis set may therefore be referred to a particular epoch, which defines the orientations of the two planes. The 'mean' equinox, ecliptic and equatorial planes, at a particular date, are the orientations obtained by neglecting the local effect of the short-period nutation of the Earth's axis of rotation. The date chosen may be either a commonly adopted epoch or the current epoch. A reference epoch given by 1 January 1950 is sometimes adopted. The frames are then defined as 'mean of 1950' or 'mean of date'. In more recent years a reference epoch of 1 Jan 2000 is generally chosen. The reference epochs are actually at noon (Universal time) on these dates. The year 2000 case is sometimes denoted 'J2000'.

A2.2 ROTATING REFERENCE FRAMES

A commonly used axis is that of a planet's rotating reference frame. The X axis is defined by the instantaneous direction from the Sun to the planet. The Y axis is in the plane of the planets orbit (which is usually close to the ecliptic), and the Z axis lies close to the ecliptic pole and completes the right-handed set. The origin is usually considered to be the centre of the planet, or could alternatively be the Sun. Such a set is shown in Figure A2.3.

A standard transformation may be obtained to transform from 'inertial' to 'rotating' axes.

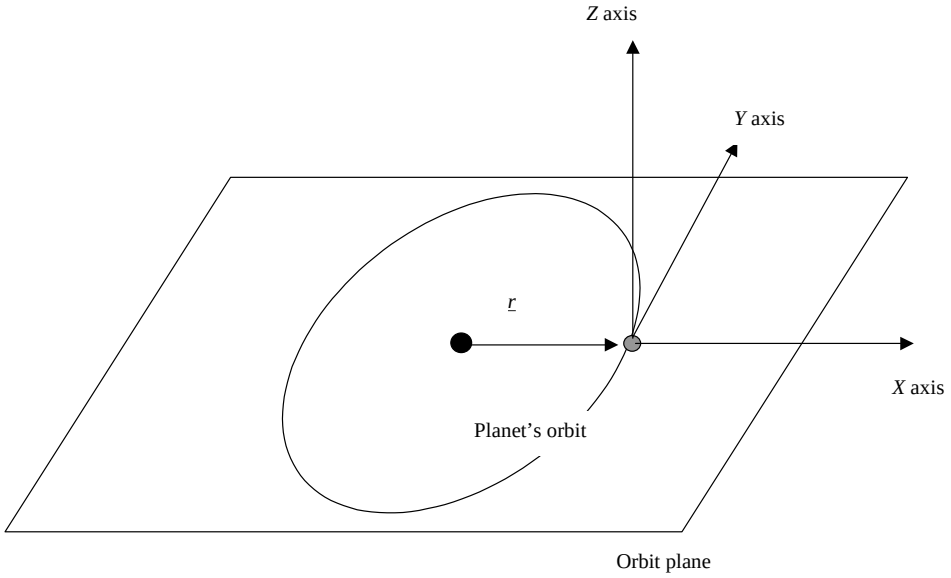

Figure A2.3. Illustration of a rotating reference plane.

The unit vector triad is obtained by:

$$\hat{x} = \frac{\underline{r}}{|\underline{r}|}, \quad \hat{y} = \frac{\underline{V} - (\hat{x} \cdot \underline{V})\,\hat{x}}{|\underline{V} - (\hat{x} \cdot \underline{V})\,\hat{x}|}, \quad \hat{z} = \hat{x} \wedge \hat{y}$$

where $\underline{r}$ and $\underline{V}$ are the Cartesian states for the position and velocity of the planet with respect to the Sun. The transformation matrix between inertial and rotating axes is so obtained:

$$[A]_I^R = [\hat{x}\hat{y}\hat{z}]$$

where A_I^R is the transformation matrix from rotating to inertial reference frames and $\hat{x}$, $\hat{y}$ $\hat{z}$ are the above triad expressed in the inertial frame.

A2.3 TIME REFERENCES

The standard unit of time is the SI unit the second. This is based on a definition based upon the time kept by atomic clocks. However, other time intervals are defined in different ways. The passage of sidereal time is defined by the hour angle of the Vernal equinox. When the meridian of the Vernal equinox is directly overhead at a point on the Earth's surface, the local sidereal time is 00:00. Greenwich sidereal time is the hour angle of the Vernal equinox with respect to the Greenwich Meridian, which is the 'prime' meridian on Earth. However, the Vernal equinox itself has alternative orientations as described in Section A2.1. Therefore, the 'true' equinox

defines the passage of 'apparent' sidereal time. The 'mean' equinox defines the passage of 'mean' sidereal time.

There are two main types of 'day'; the solar day and the sidereal day.

A sidereal day, measured by an observer on the surface of the Earth, is the interval between two successive passages of the Vernal equinox across the observer's meridian. It is a measure of the true period of the Earth's rotation about its axis, with respect to a fixed inertial reference attitude system. As in the definitions of sidereal time, both apparent and mean sidereal days are defined by the respective definitions of the equinox. The mean sidereal day is currently 86164.09054 seconds. A steady increase of approximately 0.0015 seconds per century exists. This variation is due to the steady reduction in the Earth's angular rotation rate.

The passage of solar time is defined by the hour angle of the Sun. When the Sun reaches its highest elevation seen from a point on the Earth's surface (i.e., local 'noon') the local solar time is 12:00.

A solar day, measured by an observer on the surface of the Earth, is the interval between two successive passages of the Sun's direction across the observer's meridian. However, the direction of the Sun varies by approximately one degree per day. Therefore, a solar day is slightly longer than a sidereal day. The Earth's orbit is slightly eccentric (0.0167), therefore does not travel around the Sun at a constant angular rate. Therefore, the solar day, as defined here, varies with the location of the Earth with respect to this perihelion. Therefore, an average may be taken, known as the mean solar day, being $86400 + 0.0015^{*}(\text{Year} - 1900)/100$ seconds. This steady variation in mean solar day is due to the steady state reduction in the Earth's angular rotation rate. A constant reference time is taken as the Julian day, namely 86400 seconds.

An abosolute time reference is needed. The system used is that of the Julian Date (JD). This is the number of mean solar days elapsed since noon at Greenwich on 1 Jan 4713 BC. A second absolute reference system is also used: the Modified Julian Date (MJD), which is used to allow the use of small numbers to describe current epochs.

$$\text{MJD} = \text{JD} - 2400000.5$$

Therefore, MJDs start at midnight (Greenwich local time).

The year

There are several definitions of a year. The tropical year is the period between two successive crossings of the Sun through the Vernal equinox and is 365.2422 days. This year varies from the sidereal year because of the precession of the equinoxes. A sidereal year is defined by the directions of the fixed stars and is 365.2564 days. A calendar year is 365 days except for 'leap' years with 366 days, every 4 years. This is the Julian calendar and the average length of this year is 365.25 years. The Gregorian calendar introduces an additional modification to the occurrence of leap years; one is skipped when the year is a century and is not divisible by 400. This then defines the average length of the Gregorian year as 365.2425 days (i.e., closer to othe true period of the tropical year).

Appendix 3

The planets

The nine planets of the Solar System have a spectacularly diverse set of properties. As well as inspiring scientific exploration, many of these properties influence the possibilities for mission to the planets.

The following constants and units are used:

Astronomical Unit (AU)	$1.49597870691 \times 10^{11}$ (± 3) m
Julian day (day)	86,400 secs
Julian year (year)	365.25 days
Mean Sidereal day	86,164.09054 secs = 23:56:04.09054 hours:min:sec
Sidereal year	365.25636 days
Gravitational constant	$6.67259\ (\pm 0.00030) \times 10^{-11}\,\mathrm{kg^{-1}\,m^3\,s^{-2}}$

(courtesy NASA)

A3.1 PROPERTIES OF THE PLANETS

The properties are given in Tables A3.1 to A3.4. These include the key physical properties of the planets and also the orbital data.

A3.1.1 Inner planets

Table A3.1. Physical properties of the inner planets.

	Mercury	Venus	Earth	Mars
Mass (10^{24} kg)	0.3302	4.869	5.9736	0.6419
Volume (10^{10} km^3)	6.085	92.843	108.321	16.318
Equatorial radius (km)	2,440	6,052	6,378	3,397
Polar radius (km)	2,440	6,052	6,356	3,375
Volumetric mean radius	2,440	6,052	6,371	3,390
Ellipticity	0	0	0.0034	0.0065
Mean density (kg/m^3)	5,427	5,204	5,520	3,933
Surface gravity (equatorial) (m/s^2)	3.7	8.87	9.78	3.69
Escape velocity (km/s)	4.3	10.36	11.2	5.03
GM ($\times 10^6$ km^3/s^2)	0.02203	0.3249	0.3986	0.04283
Bond albedo	0.056	0.72	0.385	0.16
Visual geometric albedo	0.11	0.65	0.367	0.15
Solar irradiance (W/m^2)	9,214	2,660	1,380	595
Black-body temperature (K)	442.5	238.9	247.3	216.6
Moment of inertia (I/MR2)	0.33	0.33	0.3308	0.366
J2 ($\times 10^{-6}$)	60	4.458	1,082.63	1,960.45

Table A3.2. Orbital data of the inner planets.

	Mercury	Venus	Earth	Mars
Semi-major axis (10^6 km)	57.9	108.2	149.6	227.9
Sidereal orbit period (days)	87.969	224.701	365.257	686.960
Perihelion (10^6 km)	46.0013	107.4760	147.0981	206.6446
Aphelion (10^6 km)	69.8171	108.9419	152.0977	249.2288
Synodic period (days)	115.88	583.92	—	779.94
Mean orbital velocity (km/s)	47.87	35.02	29.79	24.13
Sidereal rotation period (hrs)	1407.6	5832.5	23.9345	24.6229
Obliquity to orbit (deg)	~0.1	177.3	23.45	25.19
Semi-major axis (AU)	0.38709893	0.72333199	1.00000011	1.52366231
Semi-major axis rate (AU/century)	0.00000066	0.00000092	−0.00000005	−0.00007221
Orbital eccentricity	0.20563069	0.00677323	0.01671022	0.09341233
Orbital eccentricity rate (″/century)	0.00002527	−0.00004938	−0.00003804	0.00011902
Orbital inclination (deg)	7.00487	3.39471	0.00005	1.85061
Orbital inclination rate (″/century)	−23.51	−2.86	−46.94	−25.47
Longitude of ascending node (deg)	48.33167	76.68069	−11.26064	49.57854
Longitude of ascending node rate (″/century)	−446.3	−996.89	−18228.25	−1020.19
Longitude of perihelion (deg)	77.45645	131.53298	102.94719	336.04084
Longitude of perihelion rate (″/century)	573.57	−108.8	1198.28	1560.78
Mean Longitude (deg)	252.25084	181.97973	100.46435	355.45332
Mean Longitude rate (″/century)	538,101,628	210,664,136	129,597,741	68,905,103.8

A3.1.2 The outer planets

Table A3.3. Physical properties of the outer planets.

	Jupiter	Saturn	Uranus	Neptune	Pluto
Mass (10^{24} kg)	1,898.60	568.46	86.83	102.43	0.0125
Volume (10^{10} km^3)	143,128	82,713	6,833	6,254	0.616
Equatorial radius (km)	71,492	60,268	25,559	24,766	
Polar radius (km)	66,854	54,364	24,973	24,342	
Volumetric mean radius	69,911	58,232	25,362	24,624	1137
Ellipticity	0.0649	0.098	0.023	0.0171	
Mean density (kg/m^3)	1,326	687	1,318	1,638	2050
Surface gravity (equatorial) (m/s^2)	23.12	8.96	8.69	11	0.66
Escape velocity (km/s)	59.5	35.5	21.3	23.5	1.1
GM ($\times 10^6$ km^3/s^2)	126.686	37.931	5.794	6.8351	0.00083
Bond albedo	0.7	0.75	0.9	0.82	0.145
Visual geometric albedo	0.52	0.47	0.51	0.41	0.3
Solar irradiance (W/m^2)	51	15	3.71	1.47	0.9
Black-body temperature (K)	90.6	63.9	35.9	33.2	42.7
Moment of inertia (I/MR2)	0.254	0.21	0.225		
J2 ($\times 10^{-6}$)	14,736	16,298.00	3,343.43	3411	

Table A3.4. Orbital data of the outer planets.

	Jupiter	Saturn	Uranus	Neptune	Pluto
Semi-major axis (10^6 km)	778.4122	1,426.7257	2,870.9728	4,498.2538	5,906.3774
Sidereal orbit period (days)	4,335.3558	10,757.739	30,708.169	60,224.921	90,613.3324
Perihelion (10^6 km)	740.7427	1,349.4676	2,735.5556	4,459.6324	4,436.8255
Aphelion (10^6 km)	816.0816	1,503.9837	3,006.3900	4,536.8752	7,375.9294
Synodic period (days)	398.88	378.09	369.66	367.49	366.73
Mean orbital velocity (km/s)	13.07	9.66	6.82	5.48	4.75
Sidereal rotation period (hrs)	9.9250	10.500	17.24	16.11	153.2928
Obliquity to orbit (deg)	3.12	26.73	97.86	29.56	122.46
Semimajor axis (AU)	5.203363	9.53707	19.19126	30.06896	39.48169
Semimajor axis rate (AU/century)	0.000607	−0.00302	0.00152	−0.001252	−0.0007691
Orbital eccentricity	0.048393	0.054151	0.047168	0.008586	0.248808
Orbital eccentricity rate (/century)	−0.00013	−0.00037	−0.00019	0.0000251	0.00006465
Orbital inclination (deg)	1.3053	2.48446	0.76986	1.76917	17.14175
Orbital inclination rate (″/century)	−4.15	6.11	−2.09	−3.64	11.07
Longitude of ascending node (deg)	100.5562	113.715	74.22988	131.7217	110.3035
Longitude of ascending node rate (″/century)	1217.17	−1591.05	−1681.4	−151.25	−37.33
Longitude of perihelion (deg)	14.75385	92.43194	170.9642	44.97135	224.0668
Longitude of perihelion rate (″/century)	839.93	−1948.89	1312.56	−844.43	−132.25
Mean Longitude (deg)	34.40438	49.94432	313.2322	304.88	238.9288
Mean Longitude rate (″/century)	10,925078	4,401,053	1,542,548	786,449.21	522,747

The reference data commonly adopted for high-accuracy models of the ephemeris of the planets is NASA's JPL ephemeris model (courtesy NASA), available for download at http://ssd.jpl.nasa.gov/eph_info.html. These files allow the Cartesian components of planetary positions to be obtained at a given epoch, via the use of a program supplied with the model.

Less accurate data, used typically in the preliminary phases of mission design, can also be obtained from NASA. These are included in Tables A3.2 and A3.4, which contain mean orbit solutions from a 250-year least-squares fit of the NASA DE 200 planetary ephemeris to a Keplerian orbit where each element is allowed to vary linearly with time. This solution fits the terrestrial planet orbits to $\sim 25''$ or better, but achieves only $\sim 600''$ for Saturn. Elements are referenced to mean ecliptic and equinox of J2000 at the J2000 epoch (2451545.0JD = 51544.5MJD).

A3.1.3 The Sun

The key property of the Sun required in mission design is the gravitational constant:

$$1.32712440018 \times 10^{20} (\pm 8 \times 10^{9})\,\mathrm{m^3\,s^{-2}}$$

A3.2 GUIDE TO THE PLANETS

A short description of each of the planets of the Solar System is now presented, including some of the key properties of each planet and a brief history of its exploration.

A3.2.1 Mercury

Mercury is the smallest planet in the Solar System and is closest to the Sun. It has been known since prehistoric times. It is not significantly larger than Earth's Moon. The rotational period is approximately two thirds of its year, which results in extremes of surface temperatures between local noon and midnight. Temperatures reach a maximum of approximately 450°C. It has a very thin atmosphere, with a surface pressure of 10^{-15} bar (0.001 picobar), and its equator is not far removed from the ecliptic (approximately 7°).

Exploration

Mercury was explored by Mariner 10, launched by NASA in 1973. Following a Venus gravity assist to help reach Mercury, the spacecraft performed a series of three gravity assists at Mercury, affording multiple observational opportunities. NASA's Messenger is planned to reach Mercury in 2011.

A3.2.2 Venus

Venus is almost the same size as the Earth. It is often visible in the evening or early dawn. It has been known since prehistoric times. It possesses a dense atmosphere – predominantly carbon dioxide, which acts as a 'greenhouse' gas. The dense atmo-

sphere of Venus results in surface temperatures exceeding 450°C. The surface pressure is also very high, at typically 92 bar.

Venus's day is longer than its year, lasting approximately 243 days. Furthermore, its rotation is opposite to that of Earth (it is reversed when compared to the direction of its orbital motion). The obliquity of the equatorial plane to the planet's orbit is approximately 177° (compared with 23° for Earth).

Exploration

Venus has been visited several times. NASA's Mariner 2 arrived there in 1962, followed by Mariner 5 in 1967. It was then explored in greater detail by further NASA missions: Pioneer Venus and Magellan. The Pioneer Venus mission had an orbiter and also probes to enter the Venusian atmosphere. Both orbiter and probes arrived there in 1978. The probes were carried by a second spacecraft, arriving at Venus approximately five months after the orbiter's arrival, which remained in orbit until 1992, before entering the planet's atmosphere. Magellan reached Venus in 1990 and carried out a four-year mission orbiting the planet. The satellite generated radar maps of approximately 98% of the surface. The Soviet Venera series of missions visited Venus. Venera 14 deployed a lander and Venera 16 orbited in 1983. In late 2005, ESA's Venus Express mission left for Venus and plans to enter Venus orbit in the spring of 2006.

A3.2.3 Earth

Earth is the third innermost planet of the Solar System and the fifth largest. It possesses many unique features when compared with the other planets. These include the substantial presence of water on the surface, and an atmosphere with large oxygen content. No other planet is known to possess life. The obliquity of the equatorial plane to Earth's orbit is approximately 23.4°. The moon orbits Earth with a semi-major axis of approximately 384,000 km and an inclination to the ecliptic of 5°.

A3.2.4 Mars

Mars has been known since prehistoric times. The planet is relatively small, its mass being only roughly one tenth that of Earth. However, its smaller radius means that the surface gravitational acceleration is approximately one third that of Earth, giving rise to extensive speculation regarding the development of a future manned presence on Mars.

The Martian atmosphere is much thinner than that of Earth, with a surface pressure of typically 6–10 mbar. The main component of the atmosphere is carbon dioxide, at over 95%. The atmosphere does, however, extend to approximately 120 km. It can therefore be used to brake the approach of landers heading for the planet's surface. The angle between the Martian equatorial plane and the ecliptic is

similar to that of Earth. The obliquity of the equatorial plane to the planet's orbit is approximately 25°.

Exploration

Mars has attracted considerable interest as the subject of interplanetary missions. Many spacecraft have orbited the planet, and several landers have successfully reached the surface. A similar number of landers have also failed to successfully reach the surface, as planetary landing is a difficult and risk-prone task. A series of missions is planned over the next decade, and so martian exploration is set to continue.

Mars was first visited by NASA's Mariner 4, which flew by the planet in 1965. It was subsequently visited by Mariners 6, 7 and 9. The NASA Viking missions landed on the surface: Viking 1 and Viking 2 were launched within a small time interval (approximately two weeks). Each launch carried an orbiter with a lander attached. They arrived in 1976, and the landers were deployed after the landing sites were selected. The orbiter continued operations until 1980 and the landers until 1983.

The NASA Pathfinder mission was launched in 1996 and landed on Mars in 1997. The lander directly entered the atmosphere from its interplanetary approach trajectory. It also deployed a rover to explore the vicinity of the landing site. NASA later followed with two further rover missions, Spirit and Opportunity, both arriving in 2004 and with the capability to carry out long excursions across the Martian surface.

NASA used an aerobraking technique to reach the target orbit about Mars for both Mars Global Surveyor and Mars 2001 Odyssey. Surveyor arrive at Mars in 1997, and Odyssey in 2001.

Several Soviet probes have visited Mars. Phobos 2 orbited the planet in 1988.

In 2003 ESA launched Mars Express, which successfully entered orbit about Mars at the end of 2003. This mission also carried a lander named Beagle 2, but contact was lost after separation from the mother-ship.

The moons of Mars

Mars has two small moons: Phobos and Deimos, each of which is the size of a large asteroid. Both of them were discovered by Asaph Hall in 1877.

Table A3.5. The moons of Mars.

	Semi-major axis (km)	Eccentricity	Inclination (deg)	Radius (median axis) (km)	Mass (10^{15}kg)	Orbital period (days)
Phobos	9,380	0.0151	1.075	11.2	10.6	0.319
Deimos	23,460	0.0002	1.793	6.1	2.4	1.262

A3.2.5 Jupiter

Jupiter is the fifth and most massive planet in the Solar System. It has been known since prehistoric times. It is the first of the family of the outer gas giants. Its radius at a pressure of 1 bar exceeds 70,000 km. Below this radius the pressure rises rapidly. The major constituent of the Jovian atmosphere is hydrogen (90%), with significant helium content. Its equator lies close to the ecliptic, the obliquity being 3° with respect to the orbital plane. Jupiter also possesses a vast magnetosphere, which extends far into the outer Solar System. Its gravity field is so intense that orbital velocities around the planet are particularly high. This has significant implications for exploration of the atmosphere.

The major moons of Jupiter

So far, 63 Jovian moons have been discovered. The outer objects were probably asteroids captured by the Jovian gravity field. The inner moons are massive. Table A3.6 shows the four large moons orbiting within approximately 2 million km of the planet. They each have interesting individual characteristics. Io, the innermost of these moons, is volcanically active. Europa is the subject of much debate, perhaps in part inspired by science fiction novels of the last century. It is thought to possess an icy surface with an ocean below. Ganymede is the largest moon in our Solar System.

Exploration

Jupiter has been explored by several spacecraft. It was first visited by NASA's Pioneer 10, launched in 1972, which performed a gravity assist at Jupiter *en route* to the outer Solar System and beyond. Pioneer 10 has now left the Solar System and is travelling in a direction opposite to that of the Sun through the Milky Way. This probe was followed by Pioneer 11, launched in 1973. This spacecraft also performed a gravity assist at Jupiter, *en route* to Saturn and beyond.

NASA's Voyager 1 and Voyager 2 were both launched in 1977, with 1 leaving 16 days later than 2. However, Voyager 1 reached Jupiter first, in March 1979. It flew by *en route* to Saturn, and is now heading beyond the Solar System. Voyager 2 flew by Jupiter in September 1979, and continued to perform a 'grand tour' of the outer planets, passing Saturn, Uranus and Neptune.

Table A3.6. The major moons of Jupiter.

	Semi-major axis (km)	Eccentricity	Inclination (deg)	Radius (km)	Gravitational parameter ($m^3\,s^{-2}$)	Orbital period (days)
Io	421,600	0.0041	0.04	1,821	$5.960 * 10^{12}$	1.77
Europa	670,900	0.0101	0.47	1,560	$3.203 * 10^{12}$	3.55
Ganymede	1,070,000	0.0015	0.195	2,634	$9.887 * 10^{12}$	7.15
Callisto	1,883,000	0.007	0.281	2,400	$7.180 * 10^{12}$	16.69

NASA's Galileo mission was launched in 1989, reaching Jupiter after a longer transfer than the Voyagers, by performing gravity assists at Venus and Earth. It was particularly successful in exploring the planet and also its system of moons. A probe was deployed into Jupiter's atmosphere. Galileo was eventually deliberately crashed into Jupiter to avoid any potential contamination of Europa after accidental collision. Recently, Cassini flew by Jupiter on its way to Saturn.

A3.2.6 Saturn

Saturn is the sixth planet in the Solar System and the second most massive (after Jupiter). It is sometimes described as the 'jewel of the Solar System' because of its spectacular ring system. Like Jupiter, it is predominantly composed of hydrogen and helium. The equator of Saturn lies at approximately 27° from its orbital plane. Its largest moon is Titan (Table A3.7).

Exploration

The recent NASA–ESA Cassini-Huygens mission has explored the planet, its rings, and also Titan. This is the first spacecraft to orbit Saturn, as earlier visitors only flew by *en route* to the outer Solar System. The spacecraft arrived at Christmas 2004, and deployed the atmospheric probe, Huygens, which eventually descended through Titan's atmosphere.

Table A3.7. Saturn's largest moon, Titan.

	Semi-major axis (km)	Eccentricity	Inclination (deg)	Radius (km)	Gravitational parameter ($m^3\,s^{-2}$)	Orbital period (days)
Titan	1,221,800	0.0292	0.33	2,575	$8.978 * 10^{12}$	15.945

A3.2.7 Uranus

Far beyond Saturn lies Uranus, the seventh planet of the Solar System. Unlike the planets orbiting closer to the Sun, Uranus was discovered only relatively recently, by William Herschel in 1781. Uranus is another gas giant, composed of hydrogen with helium and methane as minor constituents. However, it is far less massive than Jupiter and Saturn, being approximately fifteen times the mass of Earth. One of the most unusual features of Uranus is that its equatorial plane lies at 98° from its orbital plane, and it is effectively toppled onto its side.

Exploration

Uranus was visited by Voyager 2 during its tour of the outer Solar System. The spacecraft flew by in 1986, at a distance of approximately 100,000 km

A3.2.8 Neptune

Neptune lies in the outer reaches of the Solar System. It was discovered in 1846 by Johann Gottfried Galle (based on the orbital predictions made by John Couch Adams and Urbain Leverrier). It is slightly more massive than Uranus, with a composition similar to the other gas giants. Its equator has a more conventional orientation than Uranus, lying at approximately 29° from its orbital plane. Its largest moon, Triton, is of significant interest. Several smaller moons are also present.

Exploration

Voyager 2 flew by Neptune in 1989. It is the only spacecraft to visit the planet to date.

A3.2.9 Pluto

Pluto is, on average, the most distant planet, but because of its elliptical orbit, it sometimes moves inside the orbit of Neptune. Pluto was discovered by Clyde Tombaugh in 1930. It is the smallest planet in the Solar System. It may also be the largest of a group of objects known as Kuiper belt objects. This region consists of thousands of small icy objects with diameters reaching over 1,000 km. An interesting feature of Pluto is that its orbital inclination (at 17°) is significantly higher than that of any other planet in the Solar System. This, combined with its extreme distance, makes it a difficult target for spacecraft exploration, and it has not yet been visited.

Pluto's equator also lies in an unusual attitude, at approximately 122° from its orbital plane. The planet has a very thin atmosphere composed of methane and nitrogen. It is orbited by its moon, Charon, which is more than 1,000 km in diameter and has an orbital inclination of approximately 97°.

Appendix 4

Optimising launcher injection

A4.1 LAUNCHER PERFORMANCE

Recalling Chapter 1, the maximum spacecraft mass than can be injected directly by the launcher upper stage is:

$$m_{SC} = m_0 - m_{fuel} - m_{LDry} = m_{0\max} \exp\left(\frac{-\Delta V}{Isp_L * g_0}\right) - m_{LDry}$$

where the initial mass, m_0, is always the maximum mass for the upper stage, $m_{0\max}$, if the mass of the spacecraft is to be maximised. Also m_{LDry} is the dry mass of the launcher upper stage (the mass after fuel is burnt to depletion), m_{SC} is the total mass of the spacecraft, m_0 is the initial total mass of the upper stage, and Isp_L is the specific impulse of the launcher propulsion system.

The maximum fuel tank capacity imposes a restriction on the above described performance. On reaching this limit, the required ΔV can be achieved only by reducing the mass injected in parking orbit, with implications for the achievable spacecraft mass injected into the final orbit. When the launcher upper stage is fully fuelled:

$$m_0 = \frac{m_{fuel\max}}{\left(1 - \exp\left(\frac{-\Delta V}{Isp_L * g_0}\right)\right)}$$

and therefore

$$m_{SC} = \frac{m_{fuel\max} \exp\left(\frac{-\Delta V}{Isp_L * g_0}\right)}{\left(1 - \exp\left(\frac{-\Delta V}{Isp_L * g_0}\right)\right)} - m_{LDry}$$

or $m_{SC} = m_0 - m_{fuel\max} - m_{LDry}$.

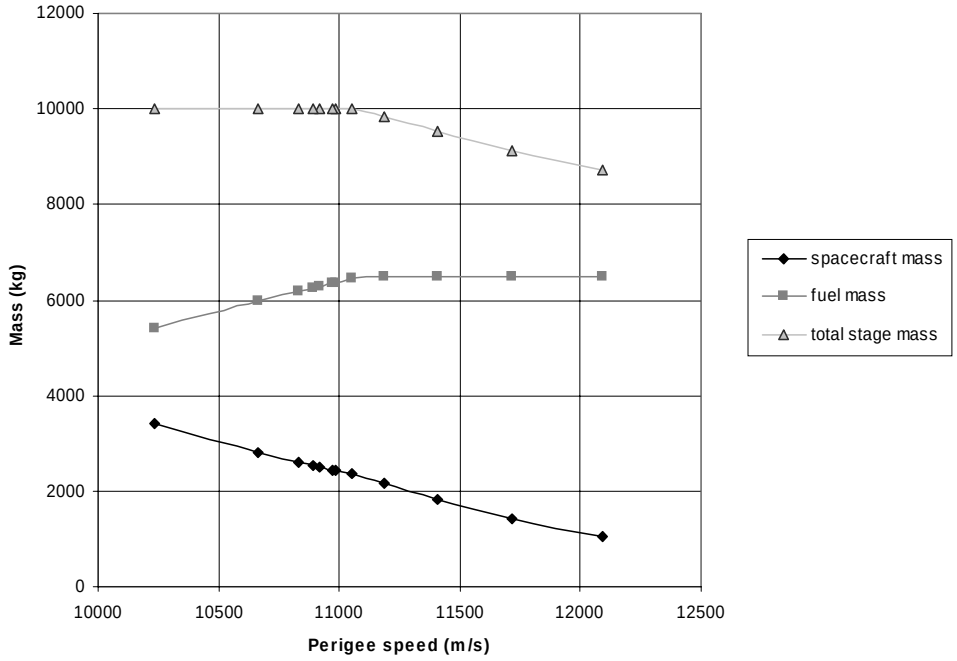

Figure A4.1. Launcher injection performance versus injection perigee speed for a tank mass capacity at 65% of upper-stage mass.

In Chapter 1 examples were given using typical intermediate launcher characteristics. This and other examples will now be considered.

In the first case, the maximum upper-stage mass that can be injected into a defined parking orbit is 10 tonnes. The parking orbit is a 200 km-altitude circular orbit. The fuel tank limit of the upper stage is assumed to be 6.5 tonnes. The dry mass of the launcher is assumed to be 1.2 tonnes.

Figure A4.1 then shows the spacecraft mass that the launcher may inject, as a function of the target perigee speed. Evaluating performance as a function of perigee speed enables a continuous plot to be achieved over the transition from bound to escape orbits. The transition occurs in this perigee altitude case at a perigee speed of approximately 11,008 m/s.

Figure A4.1 shows that the maximum upper stage mass of 10 tonnes can be fully utilised for this range of target, high-elliptical orbits (perigee speeds less than 11,000 m/s). However, at a speed of just over 11,000 m/s, the fuel-tank limit of the launcher is reached.

In the second case to be considered, the maximum upper stage mass that can be injected into a defined parking orbit is again 10 tonnes. The parking orbit is a 200-km-altitude circular orbit. The fuel tank limit of the upper stage is assumed to be 6 tonnes. The dry mass of the launcher is assumed to be 1.108 tonnes. This maintains the same dry mass-to-fuel mass ratio for the launcher. Although not a precise relationship, this is a first estimate of the dry mass dependence for such a stage.

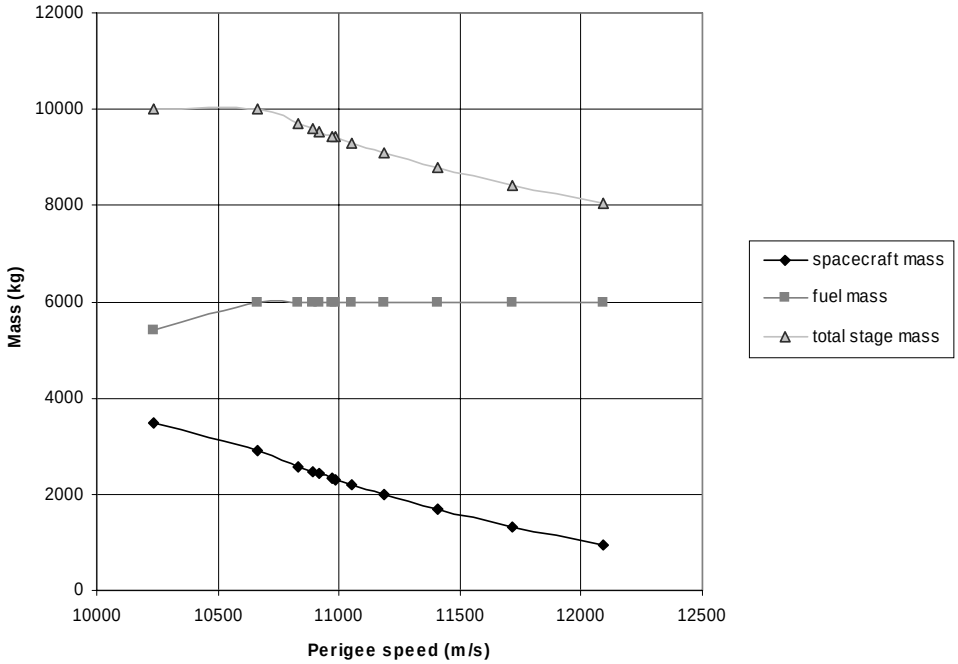

Figure A4.2. Launcher injection performance versus injection perigee speed for a tank mass capacity at 60% of upper-stage mass.

Figure A4.2 shows that the maximum upper stage mass of ten tonnes can again be fully utilised for a range of target, high apogee elliptical orbits. However, at a speed of just over 10,600 m/s, the fuel tank limit of the launcher is reached. This is lower than the case with greater fuel capacity, as it corresponds to an apogee in the region of 100,000 km.

The result is that at low-injection speeds, the spacecraft mass injected is greater than the previous case, because of the lower launcher-stage dry mass. However, at greater target speeds, the mass is lower because of the fuel mass limitations.

The procedure may be repeated for a higher fuel fraction, at 70%. The fuel tank limit of the upper stage is assumed to be 7 tonnes. The dry mass of the launcher is assumed to be 1.29 tonnes. This again maintains the same dry mass-to-fuel mass ratio for the launcher.

The result now is that at low injection speeds, the spacecraft mass injected is less than in the first case, because of the higher launcher-stage dry mass. However, at greater target speeds, the injection mass is higher. The spacecraft masses for all these cases are compared in Figure A4.4.

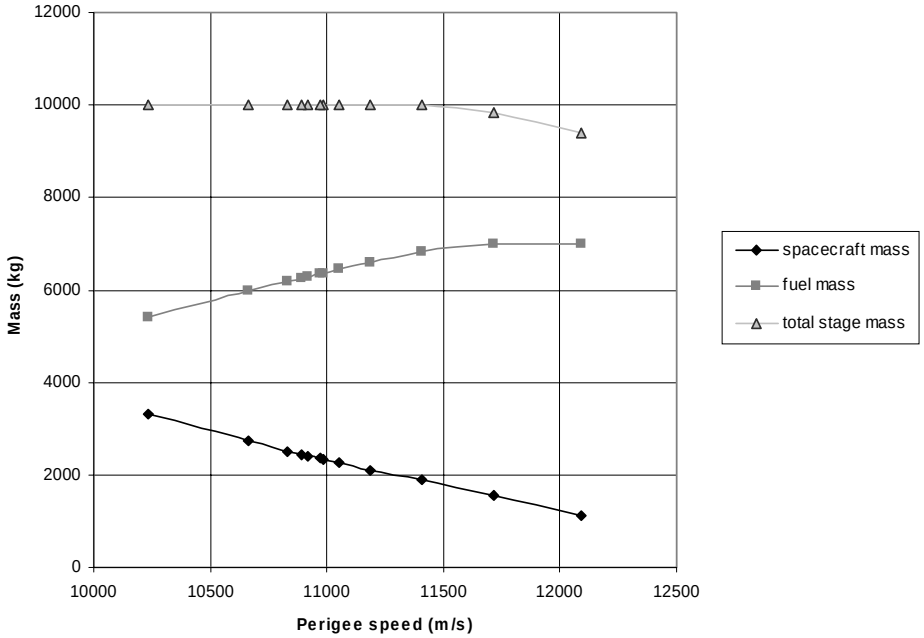

Figure A4.3. Launcher injection performance versus injection perigee speed for a tank mass capacity at 70% of upper-stage mass.

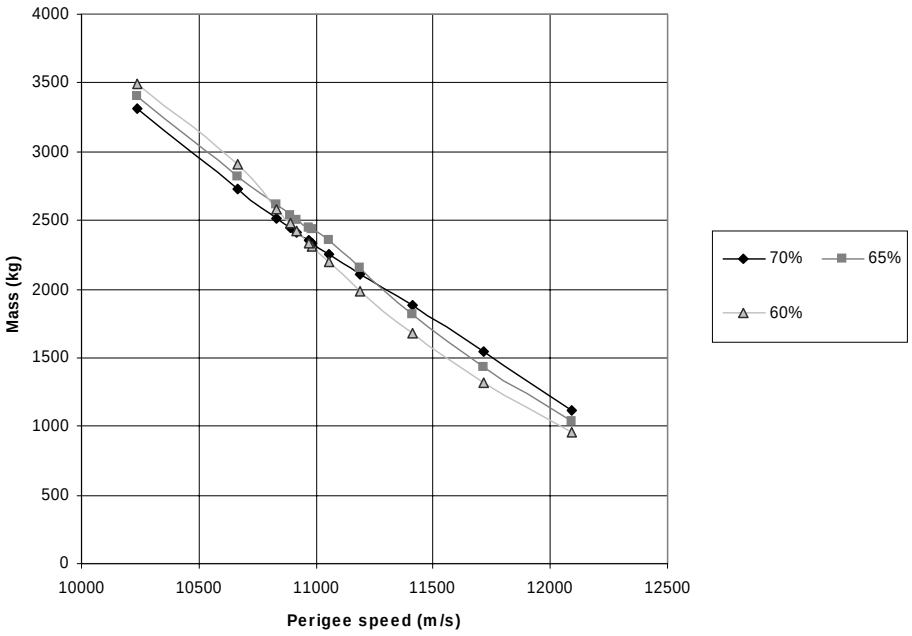

Figure A4.4. Comparative launcher injection performance versus injection perigee speed for a tank mass capacity at 60% to 70% of upper-stage mass.

A4.2 OPTIMUM INJECTION PERFORMANCE

In the case of using an intermediate injection orbit, the 'useful spacecraft mass' may be expressed by the relationships from Chapter 1 as:

$$m_{SCpay} = \left(m_0 \exp\left(\frac{-\Delta V_a}{Isp_L * g_0} \right) - m_{LDry} \right) \exp\left(\frac{-\Delta V_b}{Isp_{SC} * g_0} \right) - m_{SCprop}$$

where Isp_{SC} is the specific impulse of the spacecraft propulsion system, ΔV_a is the ΔV applied by the upper stage propulsion, and ΔV_b is the ΔV applied by the spacecraft. Each of these ΔV terms will consist of a speed change plus a loss term.

The constraint on total ΔV must apply:

$$\Delta V + \Delta V_{aLoss} + \Delta V_{bLoss} = \Delta V_a + \Delta V_b$$

The launcher injection capability for the spacecraft is then shown in Figure A4.5, for the 65% fuel capacity case. This is an extension of the previous figure (A4.1), to include lower injection perigee speeds that could be chosen for intermediate orbit injection.

This figure also shows injection at speeds beyond 11 km/sec, where escape takes place. It would not be practical to use such a launcher injection condition (i.e., escape) to an intermediate orbit, as the spacecraft manoeuvre, to reach the target escape orbit, would have to take place immediately after separation from the launch vehicle. Although possible in principle, current spacecraft design and operation

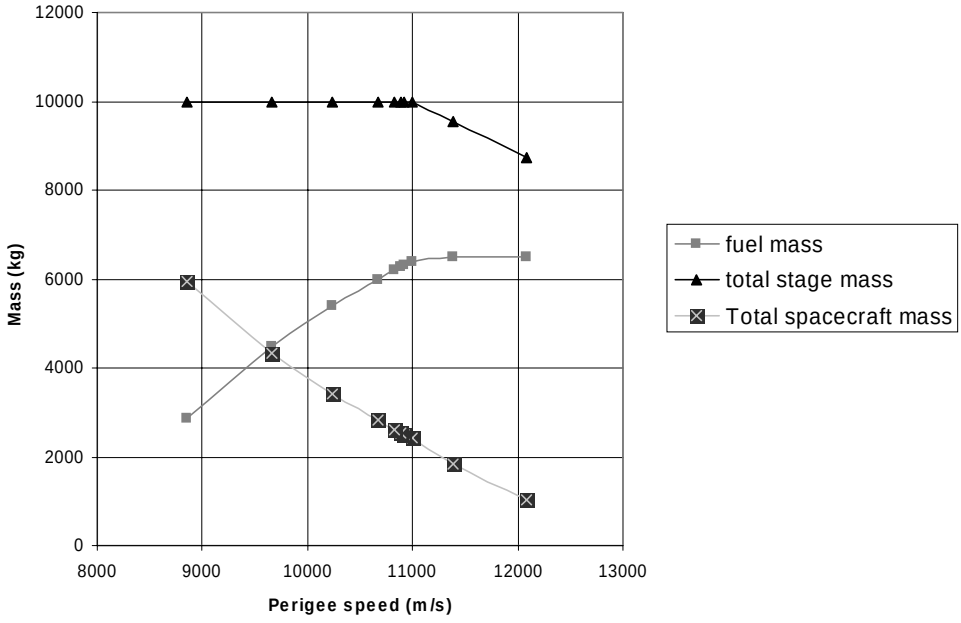

Figure A4.5. Launcher injection performance versus injection perigee speed for a tank mass capacity at 65% of upper stage mass, for use as an intermediate injection orbit.

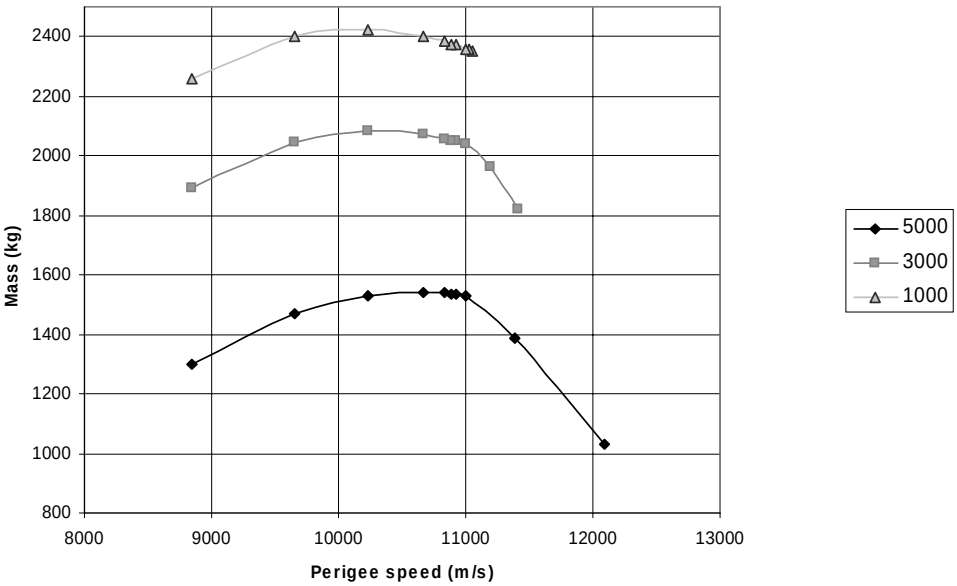

Figure A4.6. Spacecraft useful mass performance versus injection perigee speed for a launcher upper-stage tank mass capacity at 65% of upper stage mass, for three target excess hyperbolic speeds.

methods eliminate these options. However, their inclusion shows the principle of this method more clearly.

Figure A4.6 shows the useful spacecraft mass that is obtained, versus the injection perigee speed. In the following examples, the specific impulse of the spacecraft propulsion system is assumed to be lower than that of the upper stage, at 320 sec. The spacecraft propulsion mass fraction considered is 0.15. The ΔV loss assumed here is 10% in the apogee raising by the spacecraft, as this includes the escape manoeuvre that must be performed in a single burn. This manoeuvre would generally be a combination of smaller manoeuvres to raise apogee to a high elliptical orbit and then a final, larger escape manoeuvre. The 10% in this case can be regarded as average over these manoeuvres. The performance is evaluated for three target excess hyperbolic speeds, between 1 and 5 km/sec.

The figure clearly shows that the optimum injection perigee speed increases with the target excess hyperbolic speed. In the 5 km/sec case, the optimum corresponds to an intermediate orbit apogee at approximately 100,000 km (perigee speed at 10,660 m/s). The performance then falls off significantly as the injection perigee speed increases beyond the escape velocity (at 11,008 m/s). The maximum perigee speed shown in the figure, for each excess hyperbolic speed target, corresponds to a direct injection to that orbit.

The effects of variations in the launcher design should also be considered. The effects are shown in Figures A4.7 and A4.8.

When considering a given target excess hyperbolic speed, using a smaller fuel

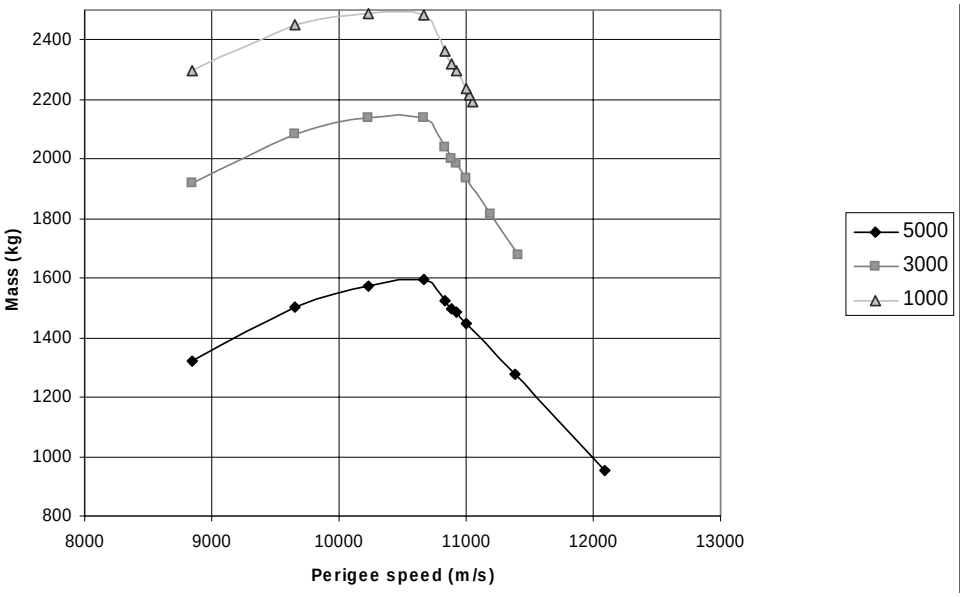

Figure A4.7. Spacecraft useful mass performance versus injection perigee speed for a launcher upper stage tank mass capacity at 60% of upper stage mass, for three target excess hyperbolic speeds.

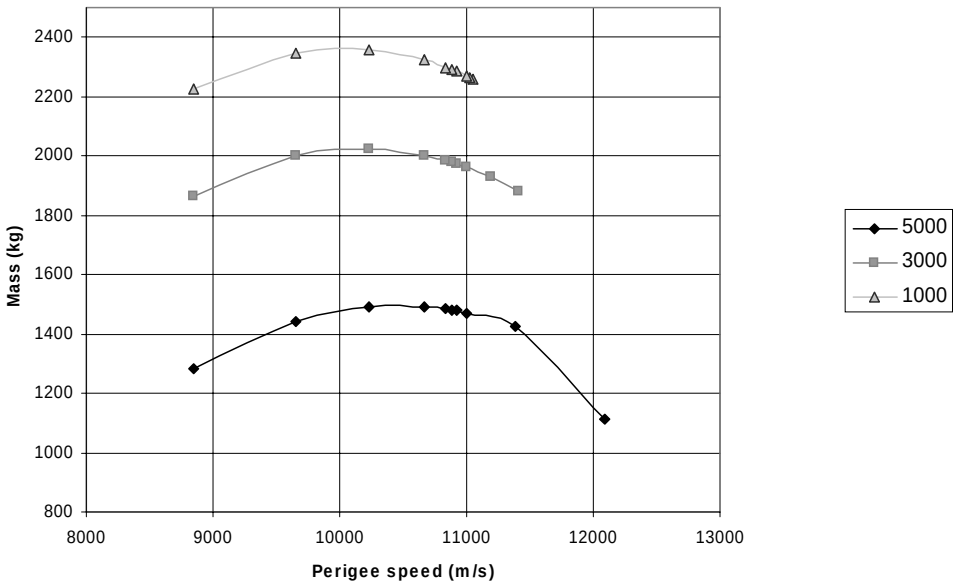

Figure A4.8. Spacecraft useful mass performance versus injection perigee speed for a launcher upper stage tank mass capacity at 70% of upper-stage mass, for three target excess hyperbolic speeds.

mass fraction in the upper stage not only penalises the direct injection performance (the performance at maximum perigee speed) but also moves the optimum injection apogee. The optimal performance capability at lower fuel fractions exceeds that at the higher fuel fraction case, because of the reduced dry mass of the upper-stage fuel tanks.

Therefore, a launcher design that enables a reduced upper-stage mass dependence on fuel mass could allow the optimal performance to switch to the higher fuel fraction case.

All cases demonstrate a significant improvement when using intermediate orbit injection, compared with a direct injection.

References and further reading

The following references provide material that is relevant to the text and that also may be read to obtain detailed information on the subjects discussed. They are divided into those that are applicable to each chapter and further sub-divided into particular subject areas within each chapter.

General

1. R.H. Battin, *An Introduction to the Mathematics and Methods of Astrodynamics* (AIAA Education series). AIAA, New York, 1987.
2. D. Brouwer, G.M. Clemence, *Methods of Celestial Methanics*. Academic Press, New York, 1961.
3. A.E. Bryson and Y.C. Ho, *Applied Optimal Control*. Hemisphere publishing corporation, 1975.
4. J.W. Cornelisse, H.F.R. Schoyer and K.F. Wakker, *Rocket Propulsion and Spaceflight Dynamics*. Pitman, London, 1979.
5. H. Goldstein, *Classical Mechanics*. Addison-Wesley, Reading, MA, 1980.
6. D.F. Lawden, *Optimal Trajectories for Space Navigation*. Butterworths, London, 1963.
7. A.E. Roy, *Orbital Motion*. Adam Hilger Co., Bristol, UK, 1982.

Orbital dynamics and data

8. R.A. Broucke and P.J.Cefola, On the equinoctial orbital elements, *Celestial Mechanics*, **5**(3), 303–310, 1972.
9. W. Donat and A. Boksenberg, *The Astronomical Almanac* (Annual publication). HMSO, London.
10. P.K. Seidelmann, *Explanatory Supplement to the Astronomical Almanac*. University Science Books, CA, 1992.
11. NASA JPL ephemeris data: *http://ssd.jpl.nasa.gov/eph_info.html*

Chapter 1

Lamberts problem

1.1. R.H. Battin, *An Introduction to the Mathematics and Methods of Astrodynamics* (AIAA Education series). AIAA, New York, 1987, pp. 276–343.
1.2. H. Shen and P. Tsiotras, Optimal two impulse rendez-vous between two circular orbits using multiple revolution Lambert's solutions. *AAS/AIAA Astrodynamics Specialist Conference, August, 1999*.
1.3. J.E. Prussing, Geometrical interpretation of angles α and β in Lambert's problem. *Journal of Guidance, Control and Dynamics*, **2**(5), 442–443, 1979.

Interplanetary missions

1.4. J.V. Breakwell, R.W. Gillespie and S.Ross, Researches in interplanetary transfer. *A.R.S.J.*, **31**, 201–208, 1961.
1.5. J. Graf, R. Zurek, R. Jones, H. Eisen, M. Johnson and B.Jai, An overview of the Mars Reconnaissance Orbiter Mission. *2002 IEEE Aerospace Conference Proceedings, Big Sky, Montana, March 11–15, 2002*.
1.6. M. Hechler and A. Yanez, *Mars Express Orbit Design*, IAC, Houston, 2002, IAC-02-A.2.09.
1.7. R.S. Saunders and G.H. Pettengill, Magellan mission summary. *Science*, **252**(5003), 247–249, April 1991.
1.8. Venus Express: *http://www.esa.int/SPECIALS/Venus_Express*

Sample return missions

1.9. R.H. Battin, The determination of round-trip planetary reconnaissance trajectories. *Journal of Aeronautical and Space sciences*, **26**, 545–567, 1959.
1.10. A.L. Friedlander, J.C. Niehoff, D.V. Byrnes and J.M. Longuski, Circulating transportation orbits between Earth and Mars. *AIAA/AAS Astrodynamics Conference, August, 1986* (AIAA 86-2009-CP).
1.11. S.J. Hoffman, J.V. McAdams and J.C. Niehoff, Round trip trajectory options for human exploration of Mars. *Greenbelt, April 1989* (AAS 89-201).
1.12. R.C. Parkinson and S. Kemble, Mars Sample Return as a Micromission. *54th IAC, Bremen, Germany, 2003* (IAC-03-Q.3.b.08).
1.13. J.R.Wertz, Interplanetary round trip mission design. *IAC, Bremen, 2003* (IAC-03-Q.4.06).
1.14. J.R. Wertz, Rapid Interplanetary round trips at moderate energy. *IAC Vancouver, 2004* (IAC-04-Q.2.a.11).

Launch vehicle performnce

1.15. Ariane V, VEGA: *http://www.arianespace.com/site/launcher/future_sub_index.htm*
1.16. Atlas, Proton: *http://www.ilslaunch.com/*
1.17. Delta2, Delta 4: *http://www.boeing.com/defense-space/space/delta/*
1.18. Dnepr: *http://www.kosmotras.ru/*
1.19. NASDA H-II: *http://www.nasda.go.jp/projects/rockets/h2a/index_e.html*
1.20. Rockot: *http://www.eurockot.com/*
1.21. Soyuz–Fregat: *http://www.starsem.com/*

Chapter 2

2.1. A. Bond, A.R. Martin, R.A. Buckland, T.J. Grant, A.T. Lawton, H.R. Mattison, J.A. Parfitt, R.C. Parkinson, G.R. Richards, J.G. Strong, G.W.Webb, A.G.A. White and P.P. Wright, Project Daedalus. *Journal of the British Interplanetary Society,* Interstellar studies, Supplement (A.R. Martin, ed.), 1978.

2.2. J.R. Brophy and M. Noca, Electric propulsion for Solar System exploration. *Journal of Propulsion and Power*, **14**(5), 700–707, 1998.

2.3. J.W. Cornelisse and H.F.R. Schoyer, K.F. Wakker, *Rocket Propulsion and Spaceflight Dynamics* (Chapter 5, pp. 85–111), Pitman, London, 1979.

2.4. D. Fearn and P. Smith, A review of UK ion propulsion a maturing technology. *IAC, Melbourne, 1998* (IAF-98-S-4.01).

2.5. R.G. Jahn, *Physics of Electric Propulsion*. McGraw Hill, New York, 1968.

2.6. J. Kawaguchi and T. Uesugi, Technology development status of the Muses C sample and return project. *IAC, Amsterdam, 1999* (IAF-99-IAA.11.2.02).

2.7. M. Leipold, M. Eiden, C.E. Garnerd, L. Herbeck, D. Kassing, T. Niederstadt, T. Krüger, G. Pagel, M. Rezazad, H. Rozemeijer, W. Seboldt, C. Schöppinger, C. Sickinger and W. Unckenbold, Solar sail technology development and demonstration. *Acta Astronautica*, **52**, 317–326, 2003.

2.8. A.E. Marini, G.D. Racca and B.H. Foing, SMART-1 Technology preparation for future planetary missions. *Advanced Space Research*, **30**(8), 1985–2000, 2002.

2.9. C.R. McInnes, *Solar Sailing: Technology, Dynamics and Mission Applications*. Springer–Praxis, Chichester, UK, 1999.

2.10. R.C. Parkinson, M. Bernasconi, P. Bravais and F. Corberand, Solar Thermal Orbit Transfer System (STOTS), *52nd IAC, Toulouse, France, Oct 2001*.

2.11. D. Poston, Nuclear design of the SAFE-400 space fission reactor. *Nuclear news*, December, 28–35, 2002.

2.12. M. Rayman, P. Varghese, D. Lehman, L. Livesay, Results from the Deep-Space 1 technology validation mission. *Acta Astronautica*, **47**, 475, 2000.

2.13. G. Saccoccia and D. Estublier, SMART-1. A technology demonstration mission for science using electric propulsion, 1998 (AIAA 98-3330).

2.14. S.S. Voss, TOPAZ II System description. *Engineering, Construction and Operations in Space IV*. Albuquerque, 1994.

2.15. H.J. Willenberg, Nuclear electric propulsion vehicle architectures, *IAC Bremen, 2003* (IAC-03.IAA.13.1.07).

Chapter 3

Optimisation methods

3.1. M.C. Bartholomew-Biggs, Recursive quadratic programming based on penalty functions for constrained minimisation, non-linear optimisation, theory and algorithms. In: L.C.W. Dixon, E. Spedicato and G.P.Szego (eds), *Numerical Optimisation Theory and Algorithms*. Birkhauser, Boston, 1980.

3.2. M.C. Bartholomew-Biggs, *Non-linear Optimisation with Financial Applications*. Boston, Kluwer, 2005.

3.3. J.T. Betts, Survey of numerical methods for trajectory optimisation. *Journal of the Astronautical Sciences*, **42**(3), 247–268, 1994.

3.4. J.T. Betts, Optimal interplanetary orbit transfer by direct transcription. *The Journal of the Astronautical Sciences*, **42**(3), 247–268, 1994.
3.5. J.T. Betts, Trajectory optimisation using sparse sequential quadratic programming. In: , R. Bulirsch, A. Miele, J. Stoer, K.H. Well (eds), *Optimal Control* (Vol 111 International series of numerical mathematics), pp 115–128. Berkhauser-Verlag, Bassel, 1993.
3.6. A.E. Bryson, Y.C. Ho, *Applied Optimal Control*. Hemisphere publishing corporation, 1975.
3.7. R. Fletcher, *Practical Methods of Optimisation,* Volume 2: *Constrained Optimisation. John Wiley and Sons, New York, 1985.*
3.8. P.E. Gill, W. Murray and M.A. Wright, *Practical Optimisation* Academic Press, New York, 1981.
3.9. T. Goodson, J. Chuang and J. Hanson, Optimal finite thrust orbit transfers with large numbers of burns. *Journal of Guidance, Control and Dynamics*, **22**(1), 139–147, 1999.
3.10. C.R. Hargraves and S.W. Paris, Direct trajectory optimisation using nonlinear programming and collocation. *Journal of Guidance, Control and Dynamics*, **10**(4), 338–342, 1987.
3.11. A.L. Herman and B.A. Conway, Direct optimisation using collocation based on high order Gauss Lobatto quadrature rules. *Journal of Guidance, Control and Dynamics*, **19**(3), 592–599, 1996.
3.12. C. Jansch, K. Schnepper and K.H Well, Ascent and Descent Trajectory Optimisation of Ariane V/Hermes. *AGARD conference proceedings No. 489, Space Vehicle Flight Mechanics*, 1989.
3.13. M. Noton, *Modern Control Engineering*. Pergamon Press, New York, 1972.
3.14. L.S. Pontryagin, V.G. Boltyanskii, R.V. Gamkrelidze and E.F. Mishchenko, *The Mathematical Theory of Optimal Processes*. Interscience, New York, 1962.
3.15. R.D. Russell and L.F. Shampine, A Collocation method for boundary value problems. *Numerical Mathematics,* **19**, 1–28, 1972.
3.16. C.G. Sauer, MIDAS: Mission Design and Analysis Software for the optimisation of ballistic interplanetary trajectories. *The Journal of the Astronautical Sciences*, **37**(3), 251–259, 1989.
3.17. W.A. Scheel and B.A. Conway, Optimisation of very low thrust multi-revolution spacecraft trajectories. *Journal of Guidance, Control and Dynamics*, **17**(6), 1265–1282, 1994.
3.18. M.Vasile, A global approach to optimal space trajectory design. *13th AAS/AIAA Space Flight Mechanics meeting, Puerto Rico, 2003* (AAS 03-141).
3.19. K.H. Well and S.R. Tandon, Rocket ascent trajectory optimisation via recursive quadratic programming. *Journal of the Astronautical Sciences*, **30**(2), 101–115, 1982.

Propulsion system optimisation

3.20. M. Auweter-Kurtz, H.L. Kurtz and H.O. Schrade, Optimisation of electric propulsion systems considering specific power as a function of specific impulse. *Journal of Propulsion*, **4**(6), 512–519, 1988.
3.21. G. Colasurdo and L. Casalino, Characteristics of electric propulsion systems for optimal interplanetary trajectories. *IAC 2003, Bremen* (IAC-03-A.7.08).
3.22. G. Fedotov, V. Kim, M. Konstantinov, V. Petukhov, G. Popov and F. Scortecci. Estimation of optimum combination of chemical upper stage and solar stationary plasma propulsion for the geostationary transfer. *IAC 1996, Beijing* (IAF96S.3.09).

3.23. L.W. Hobbs and J.P.W. Stark, Optimisation of electric propulsion for GEO missions, AIAA 1989.

Chapter 4

Motion about the Lagrange libration points and the three body problem

4.1. J.W. Cornelisse, H.F.R. Schoyer and K.F. Wakker, In: *Rocket Propulsion and Spaceflight Dynamics*. pp. 337–354. Pitman, London, 1979.
4.2. G. Gomez, J. Masdemont and C. Simo, Quasihalo orbits associated with Libration points. *The Journal of the Astronautical Sciences*, **46**(2), 135–176, 1998.
4.3. G. Gomez, A. Jorba, J.J. Masdemont and C. Simo, *Dynamics and Mission Design Near Libration Point Orbits*, Volume 4: *Advanced Methods for Collinear Points*. World Scientific, River Edge, NJ, 2001.
4.4. G. Gomez, A. Jorba, J.J. Masdemont and C. Simo, *Dynamics and Mission Design Near Libration Point Orbits*, *Advanced Methods for Triangular points*, World Scientific, River Edge, NJ, 2001.
4.5. G. Gomez, W.S. Koon, M.W. Lo, J.E. Marsden, J.J. Masdemont and S.D. Ross, Invariant manifolds, the spatial three-body problem and space mission design. *Advances in the Astronautical Sciences*, **109**, 3–22, 2001.
4.6. M. Hechler, J. Corbos and M. Bello-Mora, Orbits around L2 for First, Planck and GAIA Astronomy missions. *IAC 1999, Amsterdam* (IAF-99-A.2.02).
4.7. M. Hechler and A. Yanez, Orbits around L2 with non-gravitational perturbations. *IAC 2004, Vancouver* (IAC-04-A.7.01).
4.8. K.C. Howell, B.T. Barden and M.W. Lo, Application of dynamical system theory to trajectory design for a libration point mission. *Journal of Astronautical Sciences*, **45**(2), 161–178, 1997.
4.9. K.C. Howell and H.J. Pernicka, Station keeping for libration point trajectories. *Journal of Guidance, Control and Dynamics*, **16**(1), 151–159, 1993.
4.10. K.C. Howell and L.A. Hinday-Johnston, Time free transfers between libration-point orbits in the elliptic restricted three body problem. *Acta Astronautica*, **32**, 245–254, 1994.
4.11. A. Jorba and J. Masdemont, Dynamics of the centre manifold of the collinear points in the restricted three body problem. *Physics D*, **132**, 189–213, 1999.
4.12. W.S. Koon, M.W. Lo, J.E. Marsden and S.D. Ross, Heteroclinic connections between periodic orbits and resonant transitions. *Chaos*, **10**(2) 427–469, 2000.
4.13. W.S. Koon, M.W. Lo, J.E. Marsden and S.D. Ross, Dynamical systems, the three body problem and space mission design. In: B. Fielder, K. Groger and J. Sprekels (eds), *International Conference on Differential Equations, Berlin, 1999*, pp. 1167–1181. World Scientific, River Edge, NJ, 2000.
4.14. D.L. Richardson, A note on a Lagrangian formulation for motion about the Collinear points. *Celestial Mechanics*, **22**, 231–236, 1980.
4.15. D.L. Richardson, Analytical construction of periodic orbits about the collinear points. *Celestial Mechanics*, **22**(3), 241–253, 1980.
4.16. C. Simo, G. Gomez, J. Llibre, R. Martinez and R. Rodriquez, On the optimal station keeping control of Halo orbits. *Acta Astronautica*, **15**(6), 391–397, 1987.
4.17. C. Simo, Dynamical systems methods for space missions on a vicinity of collinear libration points. In: C. Simo (ed.), *Hamiltonian Systems with Three or More Degrees of Freedom*, pp. 223–241. Kluwer Academic Publishers, 1999.

4.18. A.E. Roy, The many body problem. In: *Orbital Motion*, pp. 111–163. Adam Hilger Co., Bristol, 1982.
4.19. G. Gómez, M.W. Lo, J.J. Masdemont (eds), Libration point orbits and applications. In: *Proceedings of the Conference Aiguablava, Spain 10–14 June, 2002*. World Scientific, River Edge, NJ, 2002.

Missions to the Lagrange libration points

4.20. R.W. Farquhar, D.P. Muhonen, C.R. Newman and H.S. Heuberger, Trajectories and orbital manoeuvres for the first Libration point satellite. *Journal of Guidance and Control*, **3**, 549–554, 1980.
4.21. R.W. Farquhar, D.P Muhonen, C.R. Newman and H.S. Heuberger, The first Libration point satellite. *AAS/AIAA Astrodynamics specialist conference*, 1979.
4.22. R.W. Farquhar and D.P. Muhonen, Mission Design for a Halo Orbiter of the Earth. *Journal of Spacecraft*, **14**(3), 170, 1977.
4.23. M. Hechler and J. Corbos, *Herschel, Plank and Gaia Orbit Design, Libration Point Orbits and Applications*. Girona, Spain, 2002.
4.24 S. Kemble, M. Landgraf and C. Tirabassi, The design of the SMART-2/LISA-Pathfinder mission, *IAC-2004*, *Vancouver* (IAC.04.A.207).
4.25. M. Landgraf, M. Hechler, and S. Kemble, Mission design for LISA Pathfinder. *Classical Quantum Gravity*, **22**, S487–S492, 2005.
4.26. M.W. Lo, B.G. Williams, W.E. Bollman, D. Han, Y. Hahn, J.L. Bell, E.A. Hirst, R.A. Corwin, P.E. Hong, K.C. Howell, B.T. Barden and R.S. Wilson, Genesis mission design. *AIAA Space Flight Mechanics* (AIAA 96-4468 1998).

Gravitational capture

4.27. E.A. Belbruno, Examples of the nonlinear dynamics of ballistic capture and escape in the Earth-Moon system. *AIAA Astrodynamics conference, Portland, August, 1990* (AIAA-90-2896).
4.28. M. Bello-Mora, F. Graziani, P. Teofilatto, C. Circi, M. Porfilio, M. Hechler, A systematic analysis on Weak Stability Boundary transfers to the Moon. *IAC 2000, Rio de Janiero* (IAF-00-A.6.03).
4.29. A. Castillo, M. Bello-Mora, J. Gonzalez, G. Janin, F. Graziani, P. Teofilatto and C. Circi, Use of Weak Stability Boundary trajectories for planetary capture. *IAC-2003, Bremen* (IAF-03-A.P.31).
4.30. K.C. Howell, B.G. Marchand and M.W. Lo, Temporary Satellite capture of short period Jupiter family comets from the perspective of dynamical systems. *AAS/AIAA Space Flight Mechanics Meeting* (AAS 00-155, 2000).
4.31. R. Jehn, S. Campagnola, D. Garcia and S. Kemble, Low-thrust approach and gravitational capture at Mercury. *18th Int. Symposium on Space Flight Dynamics, Munich, Germany, Oct, 2004*.
4.32. S. Kemble, Interplanetary missions utilising capture and escape through the Lagrange points. *IAC 2003, Bremen* (IAC-03-A.1.01).
4.33. W.S. Koon, W.S., Lo, M.W., Marsden, J.E. and S.D. Ross, Resonance and capture of Jupiter comets. *Celestial Mechanics and Dynamical Astronomy*, **81**(1–2), 27–38, 2001.
4.34. M.W. Lo and S.D. Ross, Low-energy interplanetary transfers using the invariant manifolds of L1,L2 and Halo orbits. *AAS/AIAA Space Flight Mechanics meeting, Monterey, 1998* (AAS-98-136).

4.35. S.D. Ross, Statistical theory of interior-exterior transition and collision probabilities for minor bodies on the solar system. In: G. Gomez, M.W. Lo and J.J. Masdemont (eds), *Libration Point Orbits and Applications*, pp. 637–652. World Scientific, River Edge, NJ, 2003.
4.36. F. Topputo, M. Vasile and A.E. Finzi, Combining two and three body dynamics for low-energy transfer trajectories of practical interest. *IAC 2004, Vancouver* (IAC-04-A.7.02).

Interplanetary missions with gravity assist

4.37. R.H. Battin, *An introduction to the mathematics and methods of Astrodynamics* (AIAA Education series, pp. 419–437). AIAA, New York, 1987.
4.38. S. Campagnola, R. Jehn and C. Corral, Design of Lunar Gravity Assist for the BepiColombo Mission to Mercury. *AAS 04-130, 14th AAS/AIAA Space Flight Mechanics Conference, Maui, Hawaii, Feb, 2004*.
4.39. J.M. Deerwester, Jupiter swingby missions to the Outer Planets. *Journal of Spacecraft and Rockets*, **3**(10), 1564–1567, 1966.
4.40. A.F. Heaton, N.J. Strange, J.M. Longuski and E.P. Bonfiglio, Automated design of the Europa orbiter tour (AIAA 2000-4034).
4.41. M. Lavagna, A. Povoleri and A.E. Finzi, Interplanetary mission design manoeuvre multi-objective evolutive optimisation. *IAC 2004, Vancouver* (IAC-04-A.1.02).
4.42. J.R. Johannesen and L.A. D'Amario, Europa Orbiter mission trajectory design. *AAS/AIAA Astrodynamics specialist conference, Girdwood, August, 1999* (AAS 99-360).
4.43. J.M. Longuski and S.N. Williams, Automated design of gravity assist trajectories to Mars and the outer planets. *Celestial Mechanics and Dynamical Astronomy*, **52**(3), 207–220, 1991.
4.44. J.V. McAdams and R.L. McNutt, Ballistic Jupiter gravity assist perihelion DV trajectories for an Interstellar explorer. *Journal of Astronautical Sciences*, **51**(2), 179–193, 2003.
4.45. M.A. Minovitch, Gravity thrust Jupiter orbiter trajectories generated by encountering the Galilean satellites. *Journal of Spacecraft and Rockets*, **9**, 751–756, 1972.
4.46. J.C. Niehoff, Gravity assisted trajectories to Solar System targets. *Journal of Spacecraft and Rockets*, **3**(9), 1351–1356, 1966.

Low thrust

4.47. R.H. Battin, *An introduction to the mathematics and methods of Astrodynamics* (AIAA Education series, pp. 471–490). AIAA, New York, 1987.
4.48. D. Fearn, The use of Ion thrusters for orbit raising. *Journal of British Interplanetary Society*, **33**, 129–137, 1980.
4.49. A.E. Roy, *Orbital Motion*, pp. 179–205. Adam Hilger Co., Bristol, 1982.

Low-thrust departure optimisation

4.50. M. Hechler, AGORA: asteroid rendezvous low thrust mission basic trajectory data for S/C design. European Space Operations Centre, 1983. M.A.O. working paper No. 186.
4.51. J.B. Serrano-Martinez and M. Hechler, Low-thrust asteroid rendezvous tours with Vesta. European Space Operations Centre, 1985. M.A.O. working paper No. 223.

Interplanetary missions with low thrust

4.52. L.K. Atkins, C.G. Sauer and G.A. Flandro, Solar electric propulsion combined with Earth gravity assist: A new potential for planetary exploration. *AAS/AIAA Astrodynamics specialist conference, San Diego, August, 1976* (AAS 76-807).
4.53. L. Casalino, G. Colasurdo and D. Pastrone, Optimal low-thrust escape trajectories using fly-by. *Journal of Guidance, Control and Dynamics*, **22**(5), 637–642, 1999.
4.54. L. Casalino, G. Colasurdo, D. Pastrone, Optimisation low-DV Earth gravity assist trajectories. *Journal of Guidance, Control and Dynamics*, **21**(6), 991–995, 1998.
4.55. G. Colasurdo and L. Casalino, A new mission concept to reach near Earth planets, (AIAA 2000-4137).
4.56. J. Kawaguchi, Solar electric propulsion leverage, Electric Delta-VEGA (EDVEGA) scheme and its applications. *AAS/AIAA Space Flight Mechanics meeting, Santa Barbara, CA, Feb, 2001* (AAS 01-213).
4.57. S. Kemble, Optimised Transfers to Mercury. *IAC Toulouse, 2001* (IAF-01-A.5.03).
4.58. S. Kemble and M.J. Taylor, Mission design options for a small satellite mission to Jupiter. *IAC Bremen, 2003* (IAF-03-A.09).
4.59. M. MacDonald and C.R. McInnes, Analytical control laws for near optimal geocentric solar sail transfers. *American Astronautical Society*, AAS 01-472.
4.60. H.F. Meissinger, Earth Swingby, a novel approach to interplanetary missions using electric propulsion. *AIAA 8th Electric Propulsion conference, Stanford, 1970*.
4.61. A.E. Petropoulos and J.M. Longuski, A shape based algorithm for the automated design of low-thrust, gravity assist trajectories. *AAS/AIAA Astrodynamics specialist conference, Quebec, Jul–August, 2001* (AAS 01-467).
4.62. A.E. Petropoulos, J.M. Longuski, N.X. Vinh, Shape based analytic representation of low thrust trajectories for gravity assist application. *AAS/AIAA Astrodynamics specialist conference, Girdwood, August, 1999* (AAS 99-337).
4.63. J.A. Sims, J.M. Longuski and A.J. Staugler, Vinfinity leveraging for interplanetary missions: Multiple revolution orbit techniques. *Journal of Guidance, Control and Dynamics*, **20**(3), 409–415, 1997.

Aerobraking and aerocapture

4.64. J. Beerer, R. Brooks, P. Esposito, D Lyons, W. Sidney, H. Curtis and W. Willcockson, Aerobraking at Mars: The MGS Mission. *AIAA 34th Aerospace Sciences Meeting, Reno, NV, Jan, 1996* (AIAA 96-0334).
4.65. J. R. French, Aerobraking and Aerocapture for Mars Missions, AAS 81-246.
4.66. M.Vasile, Robustness optimisation of aerocapture trajectory design using a hybrid co-evolutionary approach. *18th International Symposium on Space Flight Dynamics, October 2004, Munich*.

Chapter 5

Mission descriptions

5.1. A. Atzei, G. Schwehm, M. Coradini, M. Hechler, J. De Lafontaine and M. Eiden, Rosetta/CNSRESA's Planetary Cornerstone Mission. *ESA Bulletin*, **59**, 18–29, 1989.
5.2. A. Atzei, P. Falkner and T. Peacock, The Jovian minisat explorer: The challenge of studying Europa. *IAC Fukuoka, 2005* (IAC.05.A.3.2.A.05).

5.3. Galileo: The tour guide at: *http://www2.jpl.nasa.gov/galileo/tour*
5.4. J. Kawaguchi, Muses-C launch and early operations report. *AAS/AIAA Astrodynamics Specialists Conference, Big Sky, August, 2003* (AAS-03-662).
5.5. D. Kolbe and R. Best, The ROSETTA mission. *IAC Turin, 1997* (IAF-97-Q.5.01).
5.6. A. Lyngvi, P. Falkner, S. Kemble, M. Leipold and A. Peacock, The Interstellar Heliopause probe. *IAC Vancouver, 2004*.
5.7. A. Lyngvi, N. Rando, R. Marsden, A. Jeanes, A. Owens, L. Gerlach, G. Janin and A. Peacock. The Solar Orbiter. *IAC Fukuoka, 2005* (IAC-05-A3.2.B.07).
5.8. R T. Mitchell, The Cassini/Huygens Mission to Saturn and Titan. *Houston, October, 2002* (IAC-02-Q.2-02).
5.9. R. T. Mitchell, Cassini/Huygens at Saturn and Titan. *Fukuoka, October, 2005* (IAC-05-A3.2.A.01).
5.10. P. Renard, C. Koeck, S. Kemble, A. Atzei and P. Falkner, System concepts and enabling technologies for an ESA low-cost mission to Jupiter/Europa. *IAC Vancouver, 2004* (IAC-04-Q.2.a.02).
5.11. G. Schwehm, M. Hechler, 'Rosetta' – ESA's Planetary Cornerstone Mission. *ESA Bulletin*, **77**, 7–18, 1994.
5.12. G.D. Racca, G.P. Whitcomb and B.H. Foing, The SMART-1 Mission. *ESA Bulletin,* **95**, 72–81, 1998.
5.13. K. Uesugi, Space Odyssey of an Angel—Summary of the Hiten's Three Year Mission (AAS 93-292).
5.14. J. Van Casteren, J. Benkhoff, R. Carli, B. Gramkow, M. Novara, M. Ranne, R. Schulz, R. Jehn, BEPI COLOMBO: A mission to Mercury. *IAC Fukuoka, 2005* (IAC-05-A3.2.B.05).

Gravity assist missions

5.15. S. Cornara, M. Belló-Mora, M. Hechler, Study on Recovery of Escape Missions (AAS 03-246).
5.16. Y. Guo, R.W. Farquhar, Current design of the Solar Probe mission. *IAC Bremen, 2003,* (IAC-03-Q.2.05).
5.17. Y. Guo and R.W. Farquhar, New horizons Pluto-Kuiper belt mission: Design and simulation of the Pluto-Charon encounter. *IAC Houston, 2002* (IAC-02-Q.2.07).
5.18. Y. Langevin, Chemical and Solar electric propulsion options for a cornerstone mission to Mercury. *Acta Astronautica*, **47**(2–9), 443–452, 2000.
5.19. J.V. McAdams, Discovery class Mercury orbiter trajectory design for the 2005 launch opportunity. *AAS/AIAA Astrodynamics specialist conference, Boston, August, 1998* (AIAA 98-4283).
5.20. *http://messenger.jhuapl.edu/*
5.21. R.A. Mewaldt, J. Kangas, S.J. Kerridge and M. Neugebauer, A small probe to the heliospheric boundary and interstellar space. *Acta Astronautica*, **34**, 267–276, 1995.
5.22. SOLO: *http://www.esa.int/science/solarorbiter*
5.23. C.L. Yen, Ballistic Mercury orbiter mission via Venus and Mercury gravity assist. *Journal of the Astronautical Sciences*, **37**(3), July–Sept, 417–432, 1989.
5.24. C.L. Yen, New trajectory options for ballistic Mercury Orbiter missions (AAS 01-158).
5.25. G.J. Whiffen, An investigation of a Jupiter Galilean moon orbiter trajectory. *AAS/AIAA Astrodynamics Specialist Conference, Big Sky, August, 2003* (AAS 03-554).

Low-thrust missions

5.26. T.S. Balint, G.J. Whiffen and T.R. Spilker, Mixing moons and atmospheric entry probes: Challenges and limitations of a multi-objective science mission to Jupiter. *IAC Bremen, 2003* (IAC-03-Q.2.04).
5.27. Bepi-Colombo: *http://www.esa.int/science/bepicolombo*
5.28. G.G. Fedotov, M.S. Konstantinov and V.G. Petukhov, Electric propulsion mission to Jupiter. *47th IAC, Beijing, 1996*.
5.29. G.W. Hughes and C.R. McInnes, Mercury Sample return and small body encounters using solar sail propulsion. *IAC Houston, 2002* (IAC-02-W.2.08).
5.30. M. Katzkowski and R. Jehn, Optimum trajectories to Mercury combining low-thrust with gravity assists. *IAC Toulouse, 2001* (IAF-01-Q.2.05).
5.31. Y. Langevin, Chemical and Solar electric propulsion options for a Mercury cornerstone mission. *50th IAC, Amsterdam, 1999* (IAF-00-A.2.04).
5.32. M.Vasile, R. Biesbroek, L. Summerer, A. Galvez and G. Kminek, Options for a mission to Pluto and beyond. *AAS/AIAA Space Flight Mechanics meeting, Puerto Rico, Feb, 2003* (AAS 03-210).
5.33. M.Vasile, F. Bernelli Zazzera, R. Jehn and G. Janin, Optimal interplanetary trajectories using a combination of low-thrust and gravity assist manoeuvres. *IAC Rio de Janeiro, 2000* (IAF-00-A.5.07).

Gravitational capture

5.34. E.A. Belbruno and J. Miller, Sun-perturbed Earth to Moon transfers wilt ballistic capture. *Journal of Guidance, Control and Dynamics*, **16**, 770–775, 1993.
5.35. W.S. Koon, M.W. Lo, J.E. Marsden and S.D. Ross, Resonance and capture of Jupiter comets. *Celestial Mechanics and Dynamical Astronomy*, **81**(1), 63–73, 2001.
5.36. A. Carusi and G. Valsecchi, Numerical simulation of close encounters between Jupiter and minor bodies. In: *Asteroids*, pp. 391–416. Univ. Az. Press, Tucson, 1979.
5.37. H. Yamakawa, J. Kawaguchi, N. Ishii and H. Matsuo, A numerical study of gravitational capture orbit in the Earth-Moon system. *AAS/AIAA Spaceflight Mechanics, Colarado Springs, 1992* (AAS 92-186).

Index

Printing: Mercedes-Druck, Berlin
Binding: Stein+Lehmann, Berlin